Technical Note	1975-16
	J. L. Mannos J. L. Katz The ARIES Program: Analysis and Generation of Simulated Radar Measurements	9 July 1975

Lincoln Laboratory

MASSACHUSETTS INSTITUTE OF TECHNOLOGY
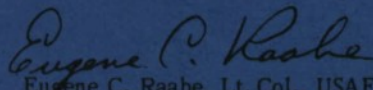
LEXINGTON, MASSACHUSETTS

This technical report has been reviewed and is approved for publication.

FOR THE COMMANDER

Eugene C. Raabe, Lt. Col., USAF
Chief, ESD Lincoln Laboratory Project Office

MASSACHUSETTS INSTITUTE OF TECHNOLOGY

LINCOLN LABORATORY

THE ARIES PROGRAM: ANALYSIS AND GENERATION OF SIMULATED RADAR MEASUREMENTS

J. L. MANNOS *

Group 67

J. L. KATZ *

Group 45

TECHNICAL NOTE 1975-16

9 JULY 1975

LEXINGTON   MASSACHUSETTS

* Formerly with Division 3.

ABSTRACT

This report describes the modeling of measurement errors in precision, long range tracking radars due to the combination of environmental effects and variations in target cross section. The environmental effects considered are tropospheric and ionospheric refraction and time delay, ionospheric scintillation, and multipath through the sidelobes at low tracking angles. In addition, radar errors due to thermal and galactic noise, equipment jitter, and bias are included. Six-degree-of-freedom vehicle dynamics are modeled to realistically represent the changing radar cross section due to target dynamics such as tumbling and precession.

CONTENTS

v

CONTENTS (Cont'd)

1.0 INTRODUCTION

ARIES is a system simulation computer program developed by Lincoln Laboratory to study radar tracking and command guided intercepts in a realistic radar environment. Written in FORTRAN and designed for execution on the CDC 6600 computer, it has considerable versatility in the specification of radar, target, tracking and environmental models.

1.1 Program Purpose

ARIES is designed to be a useful analytical tool for several allied areas. Originally ARIES was used in the strategic BMD area to estimate the metric state vector (position and velocity) of tracked targets, and then to extrapolate ahead in time to determine an intercept point for an ICBM. The radar measurements were subject to environmental effects which were reflected in the intercept miss distances. Refraction and scintillation models were used in ARIES, and the effects of various calibration schemes on target location accuracies were studied. ARIES was also used to study the problem of multipath in low angle tracking and to examine the effectiveness of various proposed schemes to overcome degradations in prediction caused by multipath. The use of ARIES in BMD studies was terminated in the summer of 1974.

More recently, a modified endoatmospheric version of ARIES, known as the HWLPTR (HOWLS Projectile Tracking Radar) Program, has been used in the tactical area for the evaluation of a radar's performance in "backtracking" an incoming artillery or mortar shell to determine its point of launch. The resulting point estimation error CEP values also assist in the evaluation of the drag model error effects and in the study of the overall performance of hostile weapon location systems.

1.2 Program Features

Since the ARIES Program provides a fairly elaborate system simulation, it is useful to tabulate the various features incorporated in ARIES. The major components of the simulation are summarized below:

1. Target trajectories---accepts input of target state vectors in several coordinate systems. Trajectories with launch angle, reentry angle or minimum energy constraints from a given launch location to an impact point are also available.

2. Radar models---both mechanically steered (dish) and phased array radars are modeled. Radar sensitivity, beamwidth, frequency and location are specified by inputs. Range and angle measurement precision are also specified by inputs.

3. Radar measurement modeling

   a. Target modeling---static cross-section measurements on real targets are used in conjunction with rigid body dynamics (Euler's

equations) to obtain realistic dynamic RCS simulations. Constant and sinusoidal, as well as an analytic cylinder, RCS options are also available.

b. Noise and propagation effects---radar measurements are corrupted by receiver noise (S/N dependent) range independent noise effects (jitter, quantization, etc.) and uncorrected propagation effects. Tropospheric and ionospheric refraction are assumed to be corrected to within random percentages (input parameters) of the true values. Ionospheric scintillation and multipath effects corrupt the data but are assumed to be uncorrected in the measurement model.

4. Trajectory estimation (Target Tracking)---Maximum Likelihood Estimation (MLE) of the target trajectory is performed based on measurement data collected at specified PRF's over specified track intervals. Individual measurements are weighted according to their measurement variances. ARIES could be easily extended to use recursive tracking algorithms.

5. Target Discrimination---(Not presently implemented.) Conceptually, discrimination algorithms would be implemented to determine whether a particular simulated target constituted a threat to the defended area.

6. Interceptor modeling---(Not presently implemented.) Flight characteristics of one or more interceptor types would be utilized to

3

conduct a command guided intercept. Currently, the program extra-
polates the estimated and true target state vectors to various time
(or altitude) points after termination of track to obtain miss
distances. Miss distance statistics are computed from the accumulated
miss distances observed on a series of Monte Carlo tests.

In addition to the above simulation components, ARIES also accommodates
multiple radars, multiple targets and multiple track intervals on a given
simulation run. The feature of making many Monte Carlo runs for a given
scenario permits the generation of meaningful miss distance statistics. A
building block/subroutine program structure lends itself to reasonable
straightforward modifications of or additions to the program.

The input/output of the ARIES Program is engineer oriented. For input,
simulation data cards are conveniently grouped into "packets" (each packet
defines a target model, a radar model, an environmental model, etc.) which
the engineer may simply stack up, together with packets specifying the desired
simulation "scenario". For output, an 8½" x 11" ARIES Test Report (see
Appendix II of Reference 1) is generated which provides the engineer with
descriptions of his input model parameters and scenarios, along with the
resultant simulation data and statistics. The outputs are all organized
into logical sections which are indexed for ready reference. Outputs from
ARIES also include trajectory plots superimposed on a world map, plots of

true and measured target cross-section, and a radar measurements tape containing metric and RCS data for processing by other programs.

1.3 Program Documentation

The ARIES Program is documented in three separate Lincoln Laboratory Technical Notes as follows:

1. The ARIES Program - A General Overview and Users' Guide

2. The ARIES Program - Coordinates, Transformations, Trajectories and Tracking

3. The ARIES Program - Analysis and Generation of Simulated Radar Measurements

The first report presents a general discussion of the ARIES Program, including the logical organization of the program and descriptions of all subroutines. All of the options available to a user are discussed and the methods of setting up the input "packets", including controls to activate the various options, are presented. A typical run, including a complete ARIES Test Report (output), is discussed in this first volume.

The second and third volumes contain all of the relevant mathematics and the models used in ARIES. Most of the deterministic mathematics (coordinate systems and transformations, trajectory generation and estimation, miss distance calculations, etc.) are in the second report. This, the third report, is primarily concerned with the generation of radar measurements,

5

including the corruptive effects of noise, radar biases, propagation and time-varying radar cross-section.

1.4 Organization of This Report

In Section 2 we start by examining the parameters and equations which are used to generate "measured" radar data for a Monte Carlo analysis. Equations are presented for both a dish type and phased array radar. Section 3 deals in more detail with random noise errors (thermal, galactic, etc.) and bias errors (quantization, etc.), and includes a description of the parameters needed to determine the signal to noise ratio (SNR). In Section 4 a model is presented for those types of atmospheric refraction which most severely affect radar performance. Both ionospheric and tropospheric refractions are considered and the proper model characteristics are provided for both day and nighttime use. It is also assumed that a given percentage of the refraction error may be corrected and a parameter to specify the amount of this residual error is provided. Section 5 is concerned with the effects of ionospheric scintillation on the signal to noise ratio and radar angle errors. A model is presented based on measurements made at M.I.T. Lincoln Laboratory Millstone Radar and earlier work by Nakagami [13]. In Section 6 multipath errors due to a second signal path reflected into the sidelobes are examined. Typical antenna sidelobe patterns and reflection coefficients are discussed along with methods for correcting the model for different mainlobe beamwidths. The last section, Section 7, is concerned with a description of the RCS

computations made by the program. Several RCS calculation techniques are presented including the use of stored static patterns, and purely mathematical models of some typical object shapes.

2.0 RADAR MEASUREMENTS

The ARIES Program makes use of a Monte Carlo technique to analyze the errors produced by a radar system. However, the use of a Monte Carlo method requires the ability to accurately simulate the radar system under test. In particular, it must be possible to simulate radar measurement errors at any point along a target trajectory. These measurement errors are obtained by corrupting the true coordinates of the target by factors depending upon the radar system parameters, signal-to-noise ratio and propagation effects. If the radar specified is an RAE tracker (dish type) then these measurements are supplied in RAE coordinates. For a phased array or RUV tracker, then the measurements are returned in RUV coordinates. In the following two sections the equations used to corrupt the true radar coordinates will be presented for the RAE and RUV cases. Detailed explanations of each term in the measurement equations may be found in the later sections which describe the development of the noise and environmental models. We start with the RAE tracker.

2.1 Radar Measurements in RAE Coordinates

For the ith trajectory point at which a measurement is desired, let $R_T(i)$, $A_T(i)$ and $E_T(i)$ represent the true range, azimuth and elevation. Then denote by $R_M(i,j)$, $A_M(i,j)$ and $E_M(i,j)$ the measured values of range, azimuth and elevation of the ith trajectory point on the jth Monte Carlo run. Note that although the true values for the RAE coordinates are the same on each Monte Carlo run, the measured values will not be, hence the need for a variable j to index the Monte Carlo run number.

8

The equations for the R, A, and E coordinate measurements are:

$$R_M(i,j) = R_T(i) \qquad\qquad\qquad\qquad\qquad (2\text{-}1)$$

$$+ \; k_1 \; \sigma_{RJ} \; RN_1(i,j) \qquad \text{Jitter}$$

$$+ \; k_2 \; \sigma_{RT}(i) \; RN_2(i,j) \qquad \text{Thermal}$$

$$+ \; k_3 \; \Delta B_R(j) \qquad\qquad \text{Bias}$$

$$+ \; k_4 \; \sigma_{RI}(i) \; RN_3(j) \qquad \text{Ionospheric refraction}$$

$$+ \; k_5 \; \sigma_{RTp}(i) \; RN_4(j) \qquad \text{Tropospheric refraction}$$

$$A_M(i,j) = A_T(i,j) \qquad\qquad\qquad\qquad\qquad (2\text{-}2)$$

$$+ \; k_1 \; \sigma_{AJ} \; RN_5(i,j) \qquad \text{Jitter}$$

$$+ \; k_2 \; \sigma_{AT}(i) \; RN_6(i,j) \qquad \text{Thermal}$$

$$+ \; k_3 \; \Delta B_A(j) \qquad\qquad \text{Bias}$$

$$+ \; k_7 \; \Delta A_{Sint} \qquad\qquad \text{Ionospheric scintillation}$$

$$E_M(i,j) = E_T(i,j) \qquad\qquad\qquad\qquad\qquad (2\text{-}3)$$

$$+ \; k_1 \; \sigma_{EJ} \; RN_7(i,j) \qquad \text{Jitter}$$

$$+ \; k_2 \; \sigma_{ET}(i) \; RN_8(i,j) \qquad \text{Thermal}$$

$$+ \; k_3 \; \Delta B_E(j) \qquad\qquad \text{Bias}$$

$$+ \; k_4 \; \sigma_{EI}(i) \; RN_9(j) \qquad \text{Ionospheric refraction}$$

$$+ \; k_5 \; \sigma_{ETp}(i) \; RN_{10}(j) \qquad \text{Tropospheric refraction}$$

$$+ \; k_6 \; \Delta E_{Mul} \qquad\qquad \text{Multipath}$$

where:

T   denotes the true or uncorrupted coordinates

M   denotes the measured or simulated coordinates

i   is an index for the track points

j   is an index for the Monte Carlo run number

k_1-k_7 are switches which are 1 if the particular form of corruption (thermal, bias, etc.) is to be used, 0 if it is to be bypassed.

$RN_n(i,j)$ are independent samples from a zero mean unit variance Gaussian random number generator. The notation $RN_n(i,j)$ is used to indicate that a new sample from the random number generator is required for each track point of each Monte Carlo run.

$RN_n(j)$ are independent samples from a zero mean unit variance Gaussian random number generator. The notation $RN_n(j)$ is used to indicate that the random number sample remains constant over the track points and changes only at the beginning of each Monte Carlo run.

The remaining parameters are described in sections 3.0 through 6.0. The table below contains a list of these parameters along with the section number where a full description is available.

Parameter	Description	Section No.
σ_{RJ}, σ_{AJ}, σ_{EJ}	Jitter errors	3.1.1
σ_{RT}, σ_{AT}, σ_{ET}	Thermal errors	3.2.1
ΔB_R, ΔB_A, ΔB_E	Bias errors	3.3.1
$VAL_n(j)$	Constant or random sample used with bias errors	3.3.1
σ_{RTp}, σ_{ETp}	Residual tropospheric refraction errors	4.3.1
σ_{RI}, σ_{EI}	Residual ionospheric refraction errors	4.3.2
ΔA_{Sint}	Ionospheric scintillation angle error	5.4
ΔE_{Mul}	Multipath elevation error	6.2

10

2.2 Radar Measurements in RUV Coordinates

For a phased array radar the measurement simulation is performed in RUV coordinates. Again, let i index the trajectory points at which a measurement is desired, and $R_T(i)$, $U_T(i)$, $V_T(i)$ denote the true values of the RUV coordinates at point i. The measured values are represented by $R_M(i,j)$, $U_M(i,j)$, $V_M(i,j)$ where j is, as in the last section, the Monte Carlo run number.

The measurement equations for the R, U and V coordinates are of a similar form to equations (2-1) to (2-3) and are as follows:

$$R_M(i,j) = R_T(i) \tag{2-4}$$

$+ k_1 \; \sigma_{RJ} \; RN_1(i,j)$	Jitter
$+ k_2 \; \sigma_{RT}(i) \; RN_2(i,j)$	Thermal
$+ k_3 \; \Delta B_R(j)$	Bias
$+ k_4 \; \sigma_{RI}(i) \; RN_3(j)$	Ionospheric refraction
$+ k_5 \; \sigma_{RTp}(i) \; RN_4(j)$	Tropospheric refraction

$$U_M(i,j) = U_T(i,j) \tag{2-5}$$

$+ k_1 \; \sigma_{UJ} \; RN_5(i,j)$	Jitter
$+ k_2 \; \sigma_{UT}(i) \; RN_6(i,j)$	Thermal
$+ k_3 \; \Delta B_U(i,j)$	Bias
$+ k_4 \; \sigma_{UTp} \; RN_7(j)$	Tropospheric refraction
$+ k_5 \; \sigma_{UI} \; RN_8(i)$	Ionospheric refraction
$+ k_6 \; \Delta U_{Mul}$	Multipath
$+ k_7 \; \Delta U_{Sint}$	Ionospheric scintillation

11

$$V_M(i,j) = V_T(i,j) \tag{2-6}$$

$$+ \ k_1 \ \sigma_{VJ} \ RN_9(i,j) \qquad \text{Jitter}$$

$$+ \ k_2 \ \sigma_{VT}(i) \ RN_{10}(i,j) \qquad \text{Thermal}$$

$$+ \ k_3 \ \Delta B_V(i,j) \qquad \text{Bias}$$

$$+ \ k_4 \ \sigma_{VTp} \ RN_{11}(j) \qquad \text{Tropospheric refraction}$$

$$+ \ k_5 \ \sigma_{VI} \ RN_{12}(j) \qquad \text{Ionospheric refraction}$$

$$+ \ k_6 \ \Delta V_{Mul} \qquad \text{Multipath}$$

$$+ \ k_7 \ \Delta V_{Sint} \qquad \text{Ionospheric scintillation}$$

where:

T denotes the true or uncorrupted coordinates

M denotes the measured or simulated coordinates

i is an index for the track points

j is an index for the Monte Carlo run number

k_1-k_7 are switches which are 1 if the particular form of corruption (thermal, bias, etc.) is to be used, 0 if it is to be bypassed.

$RN_n(i,j)$ are independent samples from a zero mean unit variance Gaussian random number generator. The notation $RN_n(i,j)$ is used to indicate that a new sample from the random number generator is required for each track point of each Monte Carlo run.

$RN_n(j)$ are independent samples from a zero mean unit variance Gaussian random number generator. The notation $RN_n(j)$ is used to indicate that the random number sample remains constant over the track points and changes only at the beginning of each Monte Carlo run.

The remaining parameters are described in sections 3.0 through 6.0. The table below contains a list of these parameters along with the section number where a full description is available.

Parameter	Description	Section No.
σ_{RJ}, σ_{UJ}, σ_{VJ}	Jitter errors	3.1.2
σ_{RT}, σ_{UT}, σ_{VT}	Thermal errors	3.2.2
ΔB_R, ΔB_U, ΔB_V	Bias errors	3.3.2
$VAL_n(j)$	Constant or random sample used with bias errors	3.3.2
σ_{RTp}, σ_{UTp}, σ_{VTp}	Residual tropospheric refraction errors	4.3.1
σ_{RI}, σ_{UI}, σ_{VI}	Residual ionospheric refraction errors	4.3.2
ΔU_{Sint}, ΔV_{Sint}	Ionospheric scintillation angle errors in U and V	5.4
ΔU_{Mul}, ΔV_{Mul}	Multipath elevation errors in U and V coordinates	6.2

2.3 Description of Measurement Generating Subroutines

The measurement equations of the preceding section are implemented predominately in subroutine MEASUR which is flowcharted in Figure 2-1. In actual use, MEASUR is called by the monitor subroutine MONITR whenever a simulated radar measurement is desired. The unerrored or true coordinates are obtained and "corrupted" by MEASUR, and these errored coordinates are returned to the track file. Also the jitter one sigma value σ_{RJ}, and thermal one sigma value $\sigma_{RT}(i)$ are combined to form a variance

13
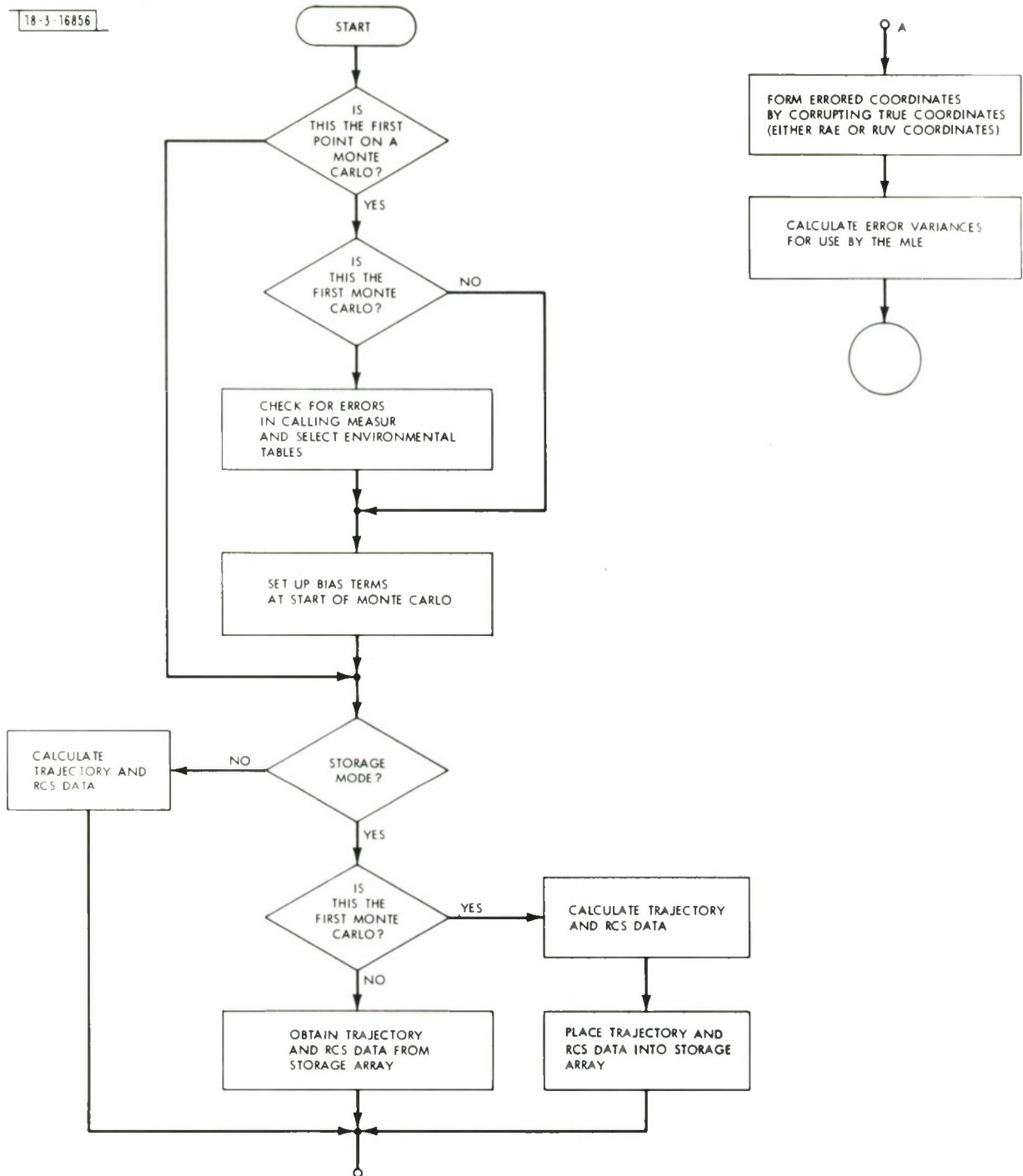
Fig. 2.1.   Flow Chart of Subroutine MEASUR.

$$\sigma^2_{Rest}(i) = \sigma^2_{RJ} + \sigma^2_{RT}(i)$$

which is supplied to the maximum likelihood estimator (MLE) at each track point i. Similar combined variances are calculated for the A and E (or U and V) coordinates and passed to the MLE.

An option is also provided to write a tape containing radar cross section data and is described in more detail in Section 7.2.

In order to conserve execution time several techniques are used. First, all multidimensional arrays are equivalenced to dummy one-dimensional arrays so that subscript calculation time would be minimized. Second, an assembly language Gaussian random generator is used instead of a Fortran version at a savings in time of 1/3 to 1/2. And finally, a storage mode option is provided to avoid the recalculation of factors such as the true RAE coordinates, radar cross section (RCS), etc., on each subsequent Monte Carlo run. This mode can be used only in those cases where the stored coordinates (R, A, E, U, V, $\dot{T}$, $\dot{E}$, RCS, and ALT (altitude)) are not varying from one Monte Carlo run to the next. Also the measurements must be required at the same point on the trajectory during each Monte Carlo run. Under these conditions a savings of approximately 25% is possible in the overall execution time.

With the exception of ionospheric scintillation and radar cross section all the errors are calculated within subroutine MEASUR. Ionospheric scintillation errors are produced by a call to subroutine ISCINT and radar cross section calculations by a call to subroutine RCS.

15

3.0 RADAR NOISE AND BIAS PARAMETERS

The types of errors modeled fall into two categories; random and bias. The random errors are due to factors such as galactic and thermal noise, receiver noise, analog to digital converter jitter, etc. These noises are uncorrelated from one measurement to the next and may or may not have time varying statistical properties. On the other hand, bias errors are considered to be those errors which remain in the system after calibration and are fixed from measurement to measurement. These include factors such as inaccurate calibration procedures, survey errors, and mechanical problems such as feed-horn sag in a dish array.

It is assumed that the various sources of bias and noise are statistically uncorrelated. This is a reasonable assumption for types of errors described in the next sections.

3.1 Jitter Errors

These are errors whose statistics do not vary as a function of the target range, although the samples at adjacent track points are considered to be uncorrelated. Typical errors of this type are the quantization errors in analog to digital converters following phase detectors or logarithmic amplifiers. Also quantization errors in devices such as shaft encoders for dish antenna angle measurements and range counters fall in this category.

Because it is not possible to accurately model the statistical distribution of these errors, a Gaussian choice is made as a reasonable approximation.

At each track point the jitter errors are considered to be zero mean with variances σ_{RJ}^2, σ_{AJ}^2, σ_{EJ}^2 for RAE coordinates, and variances σ_{RJ}^2, σ_{UJ}^2, σ_{VJ}^2 for RUV coordinates.

3.1.1 Dish Radar

If a dish radar (RAE) is selected, then σ_{RJ}, σ_{AJ}, and σ_{EJ} are input parameters read by ARIES. These parameters remain constant for all track points in the simulation. However, at each track point new random number samples are obtained from the distribution to calculate the jitter errors.

3.1.2 Phased Array Radar

For a phased array radar (RUV), σ_{RJ}, σ_{UJ} and σ_{VJ} are the jitter one sigma values read in by ARIES during execution. These parameters remain constant for all track points in the simulation. However, at each track point new random number samples are obtained from the distribution to calculate the jitter errors.

3.2 Thermal Errors

Thermal errors are used to denote noise errors whose statistics vary as a function of the target range, and which produce errors uncorrelated from one track point to the next. Examples of this type of errors are galactic noise, internal receiver noise, and clutter. To a very good approximation the

statistics of this type of noise may be represented as Gaussian with a zero mean and a given variance depending on the source of the noise.

3.2.1 Dish Radar

For the dish type radar the one sigma values for the R, A, and E coordinates are

$$\sigma_{RT}(i) = \sigma_{RT} \frac{1}{\sqrt{SNR}} \tag{3-1}$$

$$\sigma_{AT}(i) = \sigma_{AT} \frac{1}{\sqrt{SNR}} \tag{3-2}$$

$$\sigma_{ET}(i) = \sigma_{ET} \frac{1}{\sqrt{SNR}} \tag{3-3}$$

where SNR is the signal to noise ratio defined in Section 3.2.3. σ_{RT}, σ_{AT} and σ_{ET} are the reference thermal one sigma values defined at a range R_o (see SNR below) and are read by ARIES as input parameters. $\sigma_{RT}(i)$, $\sigma_{AT}(i)$ and $\sigma_{ET}(i)$ denote the thermal one sigma values at track point i.

3.2.2 Phased Array Radar

For the phased array radar the corresponding set of equations are

$$\sigma_{RT}(i) = \sigma_{RT} \frac{1}{\sqrt{SNR}}$$

$$\sigma_{UT}(i) = \sigma_{UT} \frac{1}{\sqrt{SNR}}$$

$$\sigma_{VT}(i) = \sigma_{VT} \frac{1}{\sqrt{SNR}}$$

where SNR is defined below. The remaining terms have a significance similar to their RAE counterparts above.

3.2.3 Signal to Noise Ratio

The signal to noise ratio (SNR) is defined as the ratio of signal power to noise power. In ARIES the SNR is used to multiply the reference thermal one sigma value by a factor which depends on the target range, target cross section, and ionospheric scintillation. In addition, for a phased array radar, antenna gain reduction due to scanning the beam is included.

The RAE tracker has the following expression for SNR:

$$SNR = \left(\frac{R_o}{R}\right)^4 RCS \ G^4 \qquad (3-4)$$

where

R   is the range of the target

RCS   is the left channel radar cross section of the target.

G   is the attenuation (or gain) in signal amplitude due to ionospheric scintillation. (see Section 5)

R_o is the reference range at which the SNR equals one (0 dB) for a 1 m^2 radar cross section and G=1.

19

For the RUV tracker a similar equation is obtained as:

$$SNR = \left(\frac{R_o}{R}\right)^4 RCS \ G^4 \ \cos^2\theta \qquad\qquad (3\text{-}5)$$

The R, RCS, and G terms have the same interpretation as above.

- θ is the scan angle off the phased array beam (θ=0 corresponds to a broadside beam). The $\cos^2\theta$ represents the effect of antenna gain reduction due to scanning the beam.

- R_o is the reference range for a broadside beam (θ=0) at which the SNR equals one (0 dB) for a 1 m^2 radar cross section and G=1.

3.3 Bias Errors

ARIES allows bias errors to be specified in either of two possible manners. A fixed value for the bias may be introduced which remains constant for all track points in every Monte Carlo run. Or a random number sample may be generated at the start of each Monte Carlo run, and used as the bias for all track points on that particular Monte Carlo run. On the next Monte Carlo run a new bias selection is made from the random number generator.

The first method for specifying the bias is used if it is assumed that the bias is constant for all conditions. Note that if this is in fact the case, and this constant is known, then it may be subtracted from the received data and cause no measurement errors.

The second type of bias errors results from the ability to partially correct the data by a calibration process. This type of bias error is assumed to lie in a range of values centered about the mean or true bias. From a set of measurement runs the mean can be estimated and then subtracted from the data. Thus the remaining bias may be modeled as a constant value sample function from a zero mean process which is added to the measurements at each track point. The constant value for the sample function is selected from a Gaussian distribution, since the exact form of the distribution cannot be determined.

3.3.1 Dish Radar

The bias terms for a dish radar in R, A and E coordinates are

$$\Delta B_R(j) = \sigma_{RB} \, VAL_1(j) \tag{3-6}$$

$$\Delta B_A(j) = \sigma_{AB} \, VAL_2(j) \tag{3-7}$$

$$\Delta B_E(j) = \sigma_{EB} \, VAL_3(j) \tag{3-8}$$

where σ_{RB}, σ_{AB}, and σ_{EB} are input parameters read by ARIES and

$$VAL_n(j) = \begin{cases} K - \text{for a constant bias term} \\ RN_n(j) - \text{for a bias term constant only for a given} \\ \qquad\qquad \text{Monte Carlo run} \end{cases}$$

where $RN_n(j)$ is an independent sample from a zero mean, unit variance Gaussian random number generator. The random number sample is indexed by the Monte

Carlo run number, j, to indicate that a new sample is desired each time j changes.

3.3.2 Phased Array Radar

For a phased array radar, the bias equation for range is the same as that for a dish radar. The only type of bias considered in U and V is that due to misalignment of the phased array boresight direction. The equations are

$$\Delta B_R(i) \quad = \sigma_{RB} \ VAL_1(j) \tag{3-9}$$

$$\Delta B_U(i,j) = \sigma_{UB}[\cos(AZ-A)\cos E/\cos EL]VAL_2(j) \tag{3-10}$$

$$\Delta B_V(i,j) = [\sigma_{UB}U \ \tan EL + \sigma_{VB}W]VAL_3(j) \tag{3-11}$$

where σ_{RB}, σ_{UB}, and σ_{VB} are the bias values read by ARIES as input. $VAL_n(j)$ is the same as described above for the dish radar. The bias errors at boresight are σ_{UB} and σ_{VB}. A and E are the target azimuth and elevation angles and AZ and EL are the azimuth and elevation of the phased array boresight direction. Also, $W = \sqrt{1-U^2-V^2}$.

Note that for the cases where the random number bias technique is used, three separate and independent random number samples are generated, one for each coordinate.

4.0 ATMOSPHERIC REFRACTION

An important consideration which must be taken into account in the formulation and design of any radar system is the degradation in performance resulting from propagation effects in the atmosphere. In general, the regions of the atmosphere which affect the propagation of electromagnetic waves are the troposphere and the ionosphere. The effects which are prevalent when radio waves traverse the atmosphere manifest themselves in a variety of ways. In this section, two of the phenomena in the troposphere and ionosphere which most severely effect radar systems are described as they apply to the models used in the ARIES program. In later sections other atmospheric effects will be discussed.

4.1 Atmospheric Refractivity Model

The approach taken here is summarized as follows. A standard atmospheric refractive structure for the troposphere and ionosphere is selected and this structure is assumed to be an average of prevailing conditions around the radar station. Using this atmosphere and a ray tracing computer program, the mean refraction error as a function of range and elevation angle is determined. The mean refraction error represents the contribution to the radar target position error produced by the atmosphere before any refraction correction technique is applied.

An assumption is made, however, that some statistical method is used to correct for the effects of refraction. This correction method leaves a residual error in the radar position measurement. The resulting residual error is

simulated in the ARIES program by generating a random variable whose standard deviation is some fraction of the mean refraction error. In the following sections, details of the atmospheric refractivity models are described and the method used for generating the residual error is presented.

4.1.1 Tropospheric Model

The Central Radio Propagation Laboratory (CRPL) Reference Atmosphere - 1958[7] is the model used by the ARIES Program for the troposphere. In this model, the troposphere is stratified in three layers with the refractivity in each layer defined by the Eqns. (4-1), (4-2), and (4-4).

For height, h, between $h_s \leq h \leq h_s + 1$ km the refractivity is

$$N(h) = N_s + (h - h_s)\Delta N \qquad (4-1)$$

where

$\Delta N = -7.32 \exp(5.577 \times 10^{-3} N_s)$

h_s = surface height

N_s = surface refractivity (assumed 320 N-unit for this model).

For $h_s + 1 \leq h \leq 9$ km

$$N(h) = N_1 \exp[-c(h - h_s - 1)] \qquad (4-2)$$

where

N_1 = value of N at 1 km above the surface

$$c = \frac{\ln N_1/105}{8 - h_s}, \qquad (4-3)$$

24

and for h > 9 km

$$N(h) = 105 \exp[-0.1424(h-9)].$$ (4-4)

The above model primarily depends on specifying N_s, the radio refractivity at the surface of the earth. The radio refractivity at the surface is a function of meteorological conditions at the surface and can be represented by

$$N = \frac{a}{T} (p + \frac{be}{T})$$ (4-5)

where T is the air temperature in degrees Kelvin; p, the total pressure in millibars; and e, the partial pressure of water vapor in millibars. The first term, ap/T, applies both to optical and radio frequencies, and is referred to as the dry term, while the second term, abe/T^2, is the explicit water vapor relationship required only at radio frequencies.

According to Kerr [4], the constants a and b are approximately equal to 79°K/mb and 4800°K, respectively. Campen and Cole [5] quote 74.4°K/mb and 4973°K. Through consideration of various propagation experiments, Smith and Weintraub [6] arrive at the values of 77.6°K/mb and 4810°K. The latter values for the constants a and b are the ones used in the ARIES Program.

The expression in Eqn. (4-5) for the radio refractivity is independent of frequency in the 100-MHz to 10-GHz range. According to Smith and Weintraub [6], this expression is considered to be valid to 0.5% in N units for frequencies up to 30 GHz and normally encountered ranges of temperature, pressure, and humidity.

4.1.2 Ionospheric Model

The refractive index of a medium containing free electrons is given by
Eccles and Larmor [8] as

$$n = \left[1 - \frac{N_e \, e^2}{\varepsilon_o m \, \omega^2} \right]^{\frac{1}{2}} \tag{4-6}$$

where

N_e - electron density in electrons/m^3

e - electron charge $1.6 \times 10^{-19} C$

m - electron mass 9.1×10^{-31} kg

ε_o - electric permittivity of free space 8.841941×10^{-12}

ω - angular frequency of incident wave

This relationship is valid when the earth's magnetic field and the collision
of electrons with ions and neutral particles are neglected.

The distribution of electron density with height above the earth's
surface, under equilibrium conditions, is assumed to follow the formulation
by Chapman [8] which is

$$N_e = N_m \exp \{ \tfrac{1}{2}[1 - z - \exp(-z)] \} \tag{4-7}$$

where N_m is the electron density at the maximum level of ionization and z is
the normalized height given by

$$z = \frac{h - h_m}{H} . \tag{4-8}$$

The parameters for the normalized height are h_m, the height of maximum ionization density and H, the height of the homogeneous atmosphere at a given temperature.

Using Eqns. (4-6), (4-7) and (4-8), the ionospheric refractive index is modeled by assuming a daytime ionosphere which consists of three layers (E, F_1, F_2) and a nighttime ionosphere which consists of two layers (E, F). The values for the parameters N_m, h_m and H used in the respective daytime and nighttime models are given in table 4-1.

Time	Layer	H - (km)	h_m - (km)	N_m - (electrons/m^3)
Daytime	E	10	100	1.5×10^{11}
	F_1	40	200	3.0×10^{11}
	F_2	50	300	12.5×10^{11}
Nighttime	E	10	120	0.8×10^{10}
	F	45	250	4.0×10^{11}

TABLE 4-1

PARAMETERS OF IONOSPHERIC MODEL

4.2 Refraction Errors

Using the atmospheric refractivity model described in Section 4.1, a ray tracing computer program, developed by the General Electric Co., was used to determine radar range and elevation errors. The ray tracing program computes the refractive bending which occurs as the electromagnetic wave encounters variations in atmospheric refractive index along its propagation path. From this result, the radar range and elevation errors are computed as a function of elevation angle.

Tables (4-2A), (4-3A) and (4-4A) give the range error, ε_r, and elevation error, ε_e, as a function of elevation angle used in the ARIES Program for the troposphere, daytime ionosphere and nighttime ionosphere, respectively. These tables, however, give the measurement error assuming the electromagnetic wave has passed through all of the refracting medium. For waves which pass through only part of the refracting medium, a fractional adjustment must be applied in order to obtain the error. The error for range, ΔR, and elevation, ΔE is given by

$$\Delta R = \varepsilon_r(E) \ f_1(h)$$
$$\Delta E = \varepsilon_e(E) \ f_2(h)$$

(4-9)

where f_1 and f_2 are the fractional adjustment terms given in tables (4-2B), (4-3B) and (4-4B), E is elevation angle and h is the altitude of the target. Graphs of tables (4-2), (4-3) and (4-4) are given in Figs. 4-1 to 4-3.

28

Elevation (mr)	ε_r(Elev.) (m)	ε_e(Elev.) (mr)
0.000	107.869	12.280
17.453	69.159	8.580
34.907	49.256	6.250
69.813	30.328	3.930
104.720	21.549	2.810
139.626	16.916	2.200
174.533	13.503	1.760
261.799	9.205	1.180
349.066	6.980	.870
523.599	4.816	.550
698.132	3.962	.400
872.665	3.139	.270
1047.198	2.743	.180
1221.730	2.530	.100
1396.263	2.438	.050
1483.530	2.408	.030

TABLE (4-2A)

TROPOSPHERIC ERRORS

Altitude (km)	f_1(Alt.)	f_2(Alt.)
0.0	0.000	0.000
1.0	.140	.080
2.0	.260	.140
3.0	.350	.200
6.0	.590	.330
10.0	.790	.440
20.0	.950	.600
30.0	.970	.720
60.0	.980	.830
100.0	.981	.890
300.0	.990	.940
600.0	.995	.960
1000.0	1.000	.980
5000.0	1.000	1.000

TABLE (4-2B)

TROPOSPHERIC ERROR ADJUSTMENT

Elevation (mr)	ε_r(Elev.) (m)	ε_e(Elev.) (mr)
0.000	229.880	.387
17.453	229.484	.398
34.907	228.387	.406
69.813	224.089	.413
104.720	217.566	.408
139.626	209.459	.395
174.533	200.436	.377
261.799	176.997	.325
349.066	155.631	.273
523.599	119.482	.188
698.132	100.584	.138
872.665	88.483	.101
1047.198	79.248	.071
1221.730	73.762	.045
1396.263	71.110	.021
1483.530	68.885	.010

TABLE (4-3A)

IONOSPHERIC (DAY) ERRORS

Altitude (km)	f_1(Alt.)	f_2(Alt.)
100.0	0.000	0.000
150.0	.030	.120
200.0	.090	.230
300.0	.390	.620
400.0	.750	.950
500.0	.910	1.000
700.0	.990	.960
1000.0	1.000	.890
2000.0	1.000	.780
5000.0	1.000	.600

TABLE (4-3B)

IONOSPHERIC (DAY) ADJUSTMENT

Elevation (mr)	ϵ_r(Elev.) (m)	ϵ_e(Elev.) (mr)
0.000	64.587	.116
17.453	64.465	.120
34.907	64.130	.122
69.813	62.850	.126
104.720	60.899	.125
139.626	58.491	.122
174.533	55.778	.117
261.799	48.859	.101
349.066	42.642	.085
523.599	34.138	.062
698.132	27.432	.045
872.665	23.805	.030
1047.198	21.336	.021
1221.730	20.117	.013
1396.263	19.050	.006
1483.530	18.288	.003

TABLE (4-4A)

IONOSPHERIC (NIGHT) ERRORS

Altitude (km)	f_1(Alt.)	f_2(Alt.)
100.0	0.000	0.000
150.0	.005	.030
200.0	.090	.170
300.0	.590	.820
400.0	.860	.990
500.0	.950	.990
700.0	.995	.920
1000.0	1.000	.840
2000.0	1.000	.760
5000.0	1.000	.710

TABLE (4-4B)

IONOSPHERIC (NIGHT) ADJUSTMENT
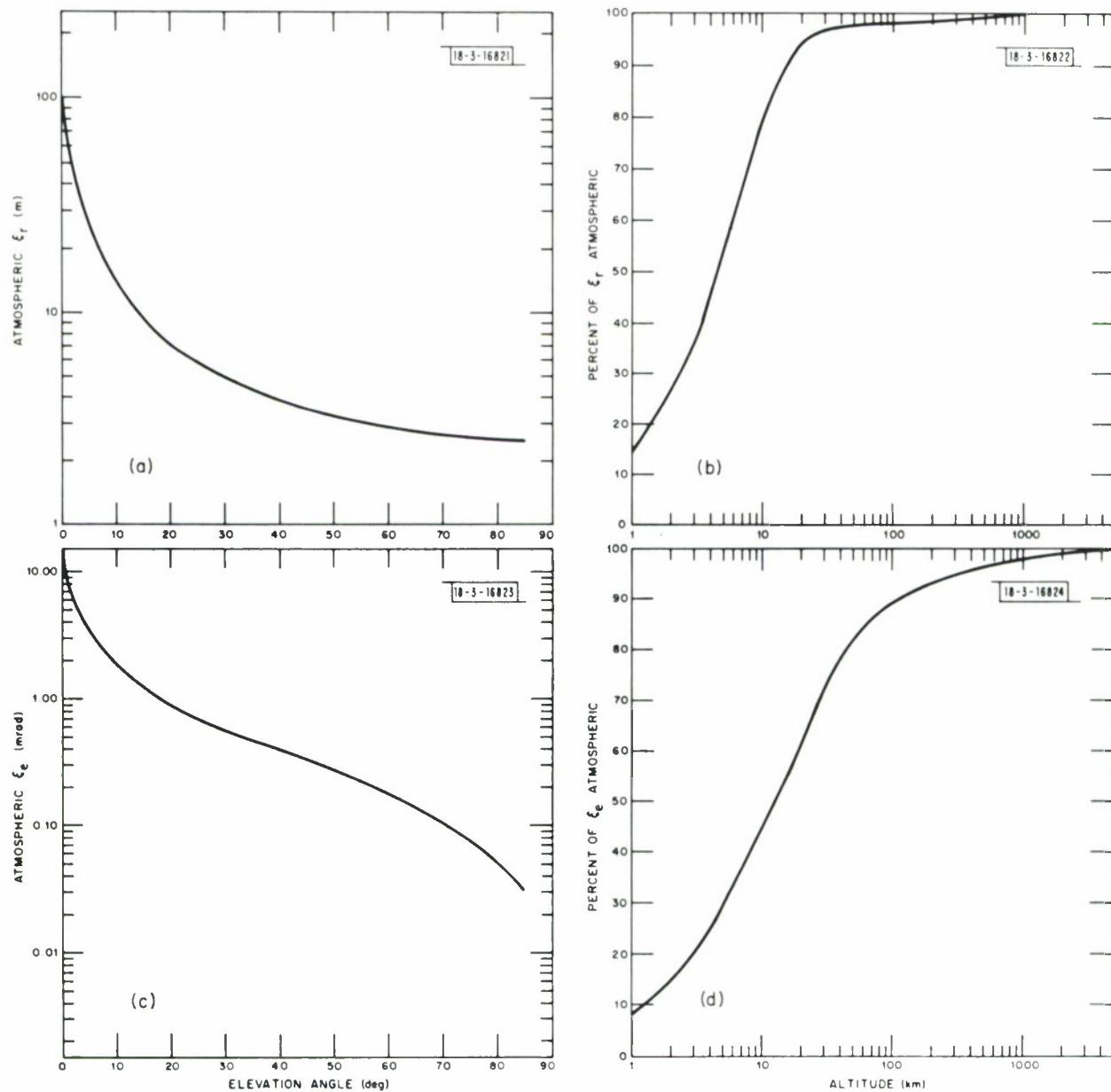
Fig. 4.1. Tropospheric induced Range Error, ε_r, and Elevation Error, ε_e, are shown as a function of elevation angle in (a) and (c). The fractional adjustment for altitude is shown in (b) and (d).

Fig. 4.2. Ionospheric Daytime induced Range Error, ε_r, and Elevation Error, ε_e, are shown as a function of elevation angle in (a) and (c). The fractional adjustment for altitude is shown in (b) and (d).

Fig. 4.3. Ionospheric Nighttime induced Range Error, ε_r, and Elevation Error, ε_e, are shown as a function of elevation angle in (a) and (c). The fractional adjustment for altitude is shown in (b) and (d).

37

4.3 Residual Error
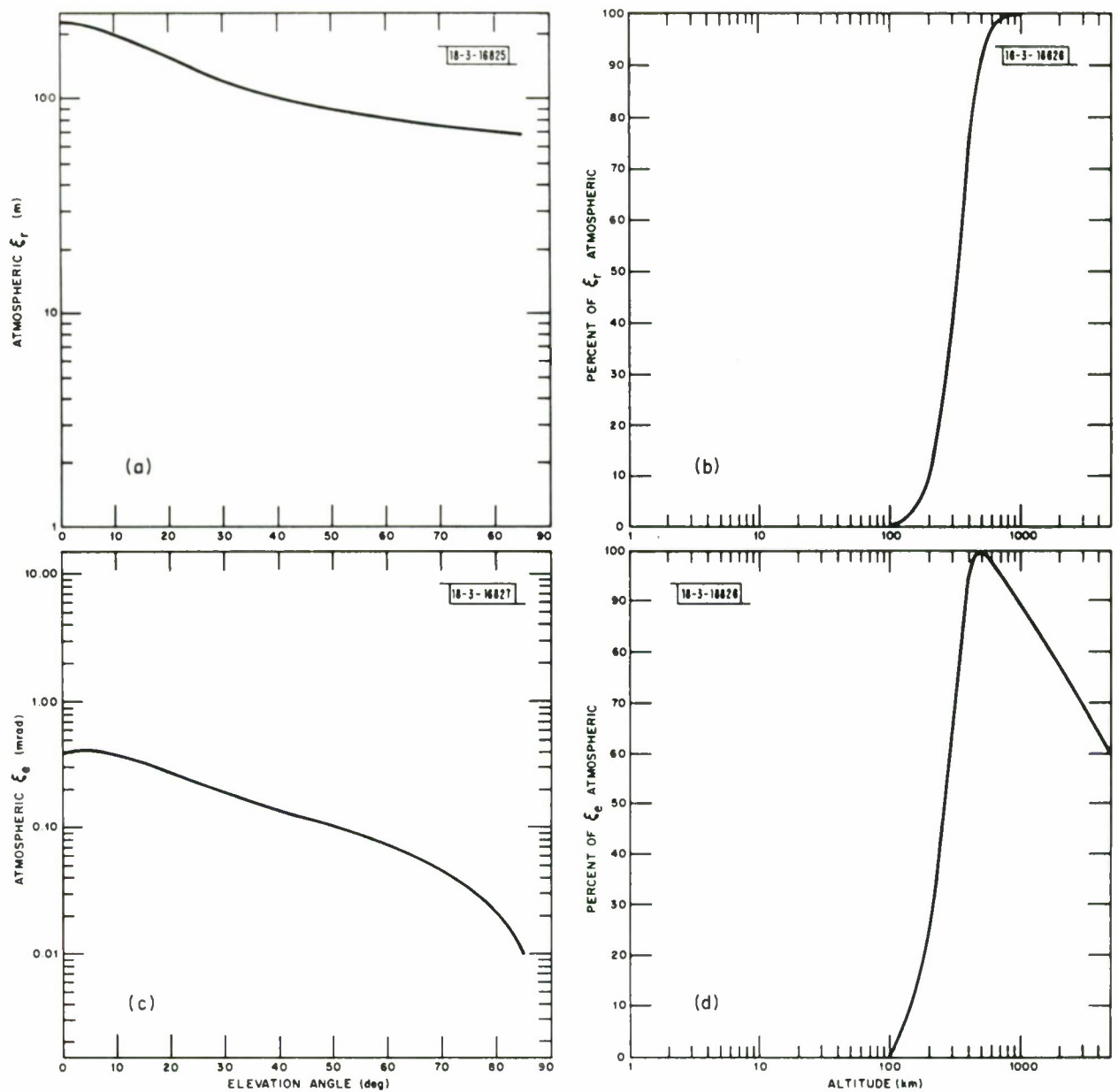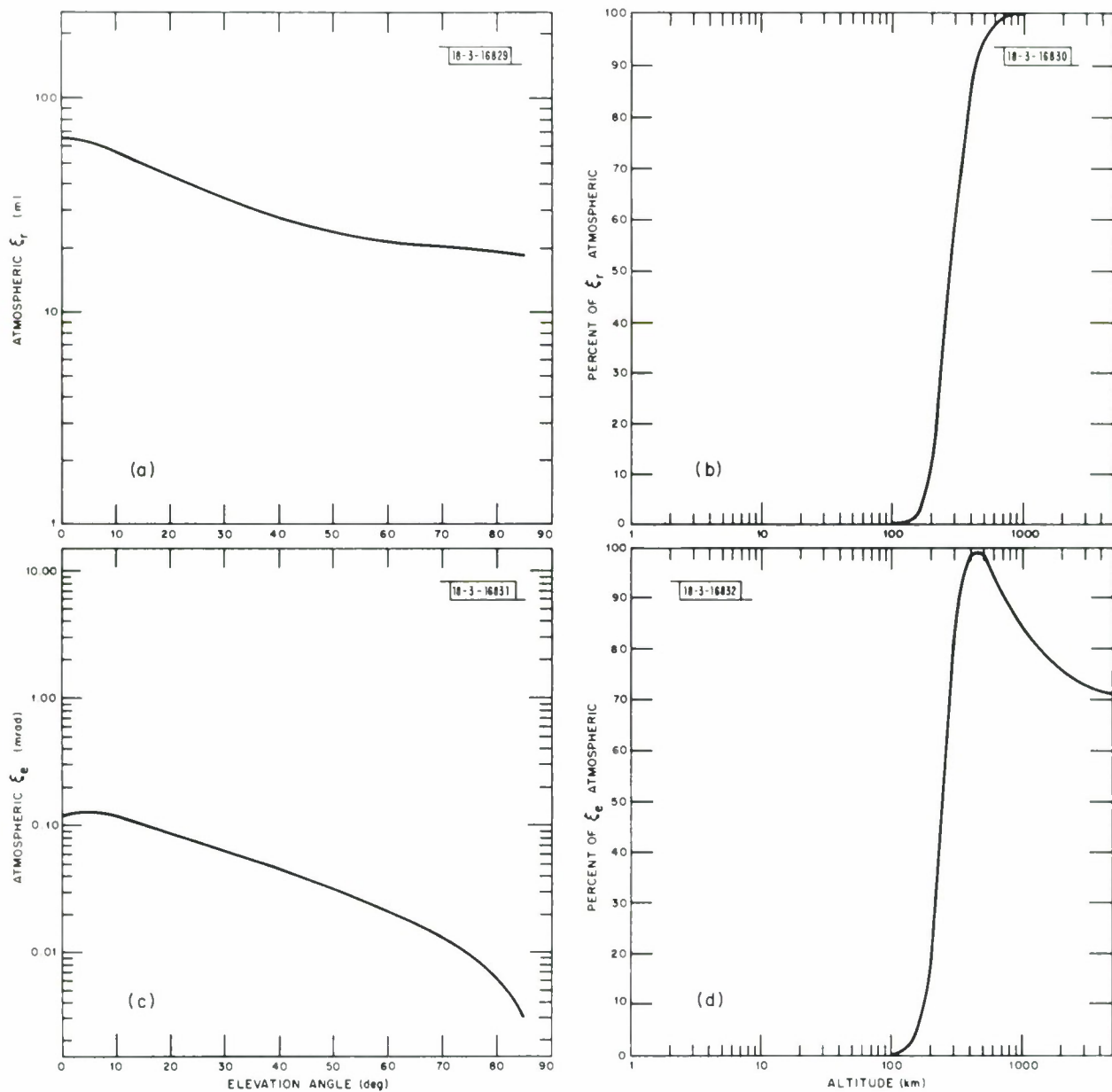
In general, the error introduced in measured target position as a result of refractive bending is random since the refractive structure of the atmosphere is not known and time varying. We assume that some statistical method, [9], [10], is used to correct for the effects of refraction which in turn produces a residual error. The resulting residual error is simulated in the ARIES program by generating a random number (for each coordinate element effected by refraction) from a distribution whose variance is related to the uncertainty in the error after the correction method is applied. The random numbers for each coordinate element are used in the measurement equations as described in Section 2.

The residual error is modeled using the following assumptions:

1. The residual error is Gaussian.

2. The refraction error obtained by table look up as described in Section 4.2 is the mean refraction error.

3. After application of a refraction correction to the radar position data, the standard deviation of the residual error is assumed to be some fraction of the absolute value of the mean refraction error.

4. We neglect azimuthal variations on the refraction terms. Azimuthal refraction arises whenever there are horizontal gradients of refractive index. Studies show, [11], that such horizontal variations are small compared to the vertical variations of the index of refraction.

38

4.3.1 Tropospheric Residual Error

Based on the assumptions in Section 4.3, the tropospheric residual error is modeled as a zero mean Gaussian process. For the ith measurement, the standard deviation of the tropospheric residual errors in RAE coordinates for range and elevation respectively are

$$
\left.
\begin{aligned}
\sigma_{RTp}(i) &= P_T \left| \Delta R_T(i) \right| \\[2ex]
\sigma_{ETp}(i) &= P_T \left| \Delta E_T(i) \right|
\end{aligned}
\right\}
\tag{4-10}
$$

where P_T is the fraction representing the uncorrectable part of the error (an ARIES input parameter) and $\Delta R_T(i)$, $\Delta E_T(i)$ are obtained from Eqn. (4-9) after using the tropospheric tables. Azimuthal refraction errors are neglected. In RUV coordinates, the standard deviation of the residual errors for the ith measurement are

$$
\left.
\begin{aligned}
\sigma_{RTp}(i) &= P_T \left| \Delta R_T(i) \right| \\[2ex]
\sigma_{UTp}(i) &= P_T \left| \sin(E)\sin(A\text{-}AZ)\Delta E_T(i) \right| \\[2ex]
\sigma_{VTp}(i) &= P_T \left| [\cos(E)\cos(EL) + \sin(E)\sin(EL)\cos(A\text{-}AZ)]\Delta E_T(i) \right|
\end{aligned}
\right\}
\tag{4-11}
$$

where

$\quad E \;\;= $ target elevation angle of the ith measurement

$\quad A \;\;= $ target azimuth angle of the ith measurement

$\quad EL = $ elevation angle of the phased array broadside

$\quad AZ = $ azimuth angle of the phased array broadside

39

4.3.2 Ionospheric Residual Error

Unlike the tropospheric model, the ionospheric model is a function of radar frequency, as can be seen by Eqn. (4-6). Tables 4-3 and 4-4 were computed based on a radar frequency of 400 MHz. For a different radar frequency, the errors (ΔR_I and ΔE_I) obtained from the tables using Eqn. (4-9) must be scaled according to the expression

$$
\left.
\begin{aligned}
\delta R_I &= \Delta R_I \, (F_0/F)^2 \\[2mm]
\delta E_I &= \Delta E_I \, (F_0/F)^2
\end{aligned}
\right\}
\qquad (4\text{-}12)
$$

where

F_0 = frequency used in generating tables 4-3 and 4-4 (400 MHz),

F = radar frequency used in simulation,

I = subscript to indicate ionospheric errors.

Based on the assumptions in Section 4.3, the ionospheric residual error is modeled as a zero mean Gaussian process. For the ith measurement, the standard deviation of the ionospheric residual errors in RAE coordinates for range and elevation respectively are

$$
\left.
\begin{aligned}
\sigma_{RI}(i) &= P_I |\delta R_I(i)| \\[2mm]
\sigma_{EI}(i) &= P_I |\delta E_I(i)|
\end{aligned}
\right\}
\qquad (4\text{-}13)
$$

where P_I is the fraction representing the uncorrectable part of the error (an ARIES input parameter) and $\delta R_I(i)$, $\delta E_I(i)$ are obtained from Eqns. (4-9) and

40

(4-12). Azimuthal refraction errors are neglected. In RUV coordinates the standard deviation of the residual errors for the ith measurement are

$$\sigma_{RI}(i) = P_I |\delta R_I(i)|$$

$$\sigma_{UI}(i) = P_I |\sin(E)\sin(A\text{-}AZ)\delta E_I(i)|$$

$$\sigma_{VI}(i) = P_I |[\cos(E)\cos(EL) + \sin(E)\sin(EL)\cos(A\text{-}AZ)]\delta E_I(i)|$$

(4-14)

where all parameters have been defined in Section 4.3.1.

5.0 IONOSPHERIC SCINTILLATION

The ionospheric scintillation model was developed by R. H. Wand [12] from UHF measurements made at M.I.T. Lincoln Laboratory, Millstone Radar Site, over the period from 1971 to 1973. Two forms of the model are considered, a "0.1% probability model" and a "worst case ever model". For the first model, the level of scintillation specified could be expected to be exceeded only about .1% of the time for a radar operating in or near the auroral zone. The second model is based on measurements made at Millstone Hill during a period of severe magnetic disturbances (Kp = 8+) which were the largest fluctuations ever observed during the Millstone satellite tracking program. As a comparison the worst case ever model represents a level of scintillation approximately four times larger than the .1% probability model.

5.1 Ionospheric Scintillation Model

Theoretical and experimental considerations indicate that the amplitude fluctuations produced by ionospheric scintillation may be represented as a function of samples drawn from a Nakagami M-distribution [13]:

$$f_M(B) = \frac{2M^M \, B^{2M-1} \, e^{-MB^2}}{\Gamma(M)} \qquad \begin{array}{l} B \geq 0 \\ M \geq \frac{1}{2} \end{array} \qquad (5-1)$$

where the parameter $M = (2\sigma_G)^{-2}$ and σ_G, the rms amplitude fluctuation, is obtained from the orbital geometry in a manner which will be explained shortly. Then if $\bar{A}$ represents the mean of the signal amplitude (i.e., the amplitude if

no scintillation were present), and if A represents the received signal amplitude with scintillation, we have

$$A = G^2 \bar{A} \qquad (5\text{-}2)$$

where

$$G = (1 + \sigma_G)B^2 \qquad (5\text{-}3)$$

and B is drawn from the distribution in (5-1). The G term in Eqn. (5-2) which represents the gain or attenuation in amplitude due to the scintillation is squared because the radar measurement is a two-way transmission.

We obtain σ_G, the rms amplitude fluctuation, as:

$$\sigma_G = \sigma_0 (\tfrac{z}{h} \sec i)^{\frac{1}{2}} \qquad (5\text{-}4)$$

where

$$\sigma_0 = \begin{cases} .04 \text{ for the ''0.1\% probability model''} \\ .16 \text{ for the ''worst case ever model''} \end{cases}$$

and

$$z = \frac{z_1 z_2}{z_1 + z_2} \qquad (5\text{-}5)$$

where z_1, z_2, and h are defined in Fig. 5-1. The zenith angle i at the irregularities is obtained from

43

$$i = \sin^{-1}\left(\frac{r_o \cos E}{r_o + h}\right) \qquad (5\text{-}6)$$

where r_o is the earth's radius. Note that the above equation applies only for $z_2 > 0$. σ_G should be made zero once the RV target penetrates the layer of irregularities. Also, if Eqn. (5-5) yields a value of $\sigma_G > .5$, then we should set $\sigma_G = .5$.

A given value of B in (5-2) is held for a correlation time τ which corresponds roughly to the time taken for the penetration point at height h to traverse a "typical" ionospheric irregularity. In general, a mixture of irregularity scale sizes are present, but the size which is most prominent in producing the amplitude scintillations has a radius of one Fresnel zone, $\sqrt{\lambda z}$, where λ is the observing wavelength. Then

$$\tau \approx \frac{\sqrt{\lambda z}}{|V_p|} \qquad (5\text{-}7)$$

where the effective penetration point speed V_p is given by

$$V_p = \frac{z_1}{z_2}(z_1 + z_2)(\dot{E}^2 + \dot{T}^2)^{\frac{1}{2}} \qquad (5\text{-}8)$$

and $\dot{E}$ and $\dot{T}$ are the rate of change of elevation and traverse angle respectively in radians/sec. If the RV is moving in such a manner that V_p is small, then a minimum value of 100 m/sec is assumed, corresponding to the speed of the most probable size irregularity.
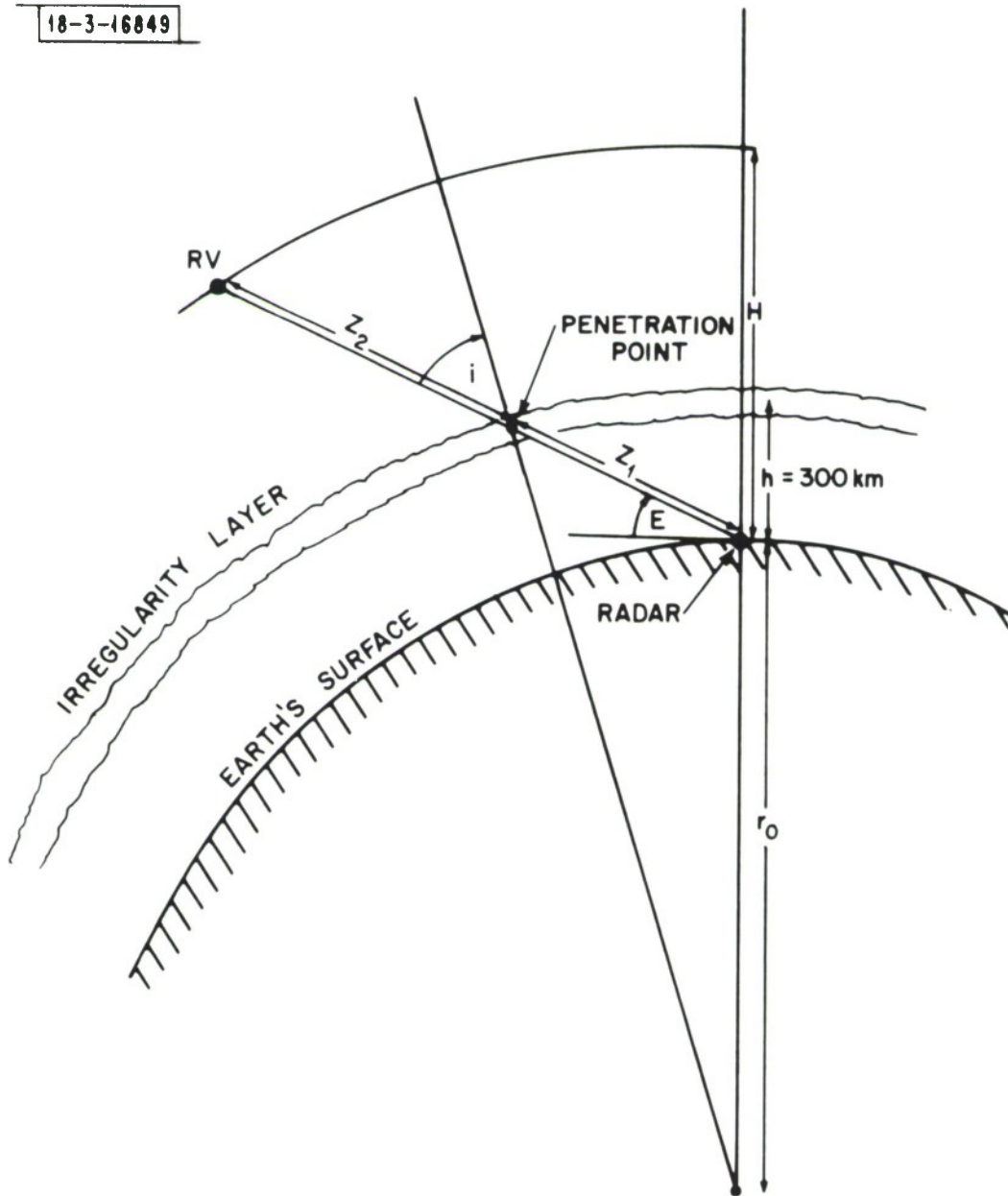
Fig. 5.1. Ionospheric Scintillation Model.

45

For the effects of the ionospheric scintillation on angle measurements we first note that UHF observations at Millstone Hill showed that angle scintillation was generally much more pronounced in traverse angle than in elevation angle. This is presumably related to the high inclination angle of the earth's magnetic field and the fact that the irregularities are elongated in the direction of the field. The UHF results also gave approximately a linear relationship between rms amplitude scintillation fluctuations and the rms fluctuation in traverse angle σ_T.

$$\sigma_T = 40 \ \sigma_G \ \text{mdeg} \tag{5-9}$$

Hence Eqn. (5-9) provides a means of predicting a model value for σ_T using the model value of σ_G. The fluctuations in elevation angle produced by ionospheric irregularities will be neglected.

The probability distribution of traverse angle fluctuations may be taken as Gaussian, $N(0, \ \sigma_T)$, while the correlation time may be assumed to be the same as for amplitude fluctuations, Eqn. (5-7). No adjustment to the traverse angle fluctuation is necessary to allow for the two-way path involved in a radar situation.

5.2 Generation of Nakagami-M Random Numbers

The Nakagami-M-distributed random variable B of Eqn. (5-1) is generated in subroutine NAKGMI by one of three possible methods depending on the value of M.

46

For M > 15 a Gaussian approximation to the Nakagami-M distribution is used which is of the form

$$B = \{1 + 1/9M + (1/9M)^{\frac{1}{2}}RN\}^{3/2}$$

where RN is an N(0,1) Gaussian random variable.

For $3 \leq M < 15$ a transformation of uniform random variables is used. Let $\{U_i\}$ be independent uniformly distributed random variables over the interval (0,1). Then for M an <u>integer</u>,

$$B_{int} = \sqrt{-\frac{1}{M} \log \left(\prod_{i=1}^{M} U_i \right)} \qquad (5\text{-}10)$$

will be distributed as a Nakagami-M random variable. If M is not an integer we form M_{int} as

$$M_{int} = \lfloor M \rceil$$

where $\lfloor \cdot \rceil$ represents the closest integer value and then form B as

$$B = \frac{B_{int} - a}{b}$$

where B_{int} is generated by setting $M=M_{int}$ in equation (5-10) and where

$$b = \sqrt{1 - \frac{\Gamma(M_{int} + \frac{1}{2})}{(M_{int})^{\frac{1}{2}} \Gamma(M_{int})} \Big/ 1 - \frac{\Gamma(M + \frac{1}{2})}{M^{\frac{1}{2}} \Gamma(M)}}$$

47

$$a = \frac{\Gamma(M_{int} + \frac{1}{2})}{(M_{int})^{\frac{1}{2}}\Gamma(M_{int})} - b\frac{\Gamma(M)}{M^{\frac{1}{2}}\Gamma(M)}$$

The technique works by transforming the distribution of the closest integer, M_{int}, so that it has the same mean and variance as the desired Nakagami-M distribution. This method successfully passed a χ^2-test on its density function for values of M between 2 and 35. As a safety precaution this technique is not used for M < 3 in ARIES. For M > 15 the Gaussian approximation is used because it requires less execution time.

For .5 ≤ M ≤ 3 a probability integral transformation [14] is used. Let

$$F(X) \triangleq \int_0^X f_M(\beta)d\beta \tag{5-11}$$

be the distribution function for the Nakagami-M density function of Eqn. (5-1). Because Y = F(X) is a monotone increasing function for X ≥ 0 then

$$X = F^{-1}(Y) \qquad 0 \le Y \le 1 \tag{5-12}$$

where F^{-1} is used to denote the inverse of F. If we select a Y which is uniformly distributed from 0 to 1, then by the probability integral transformation, X will be seen to be a Nakagami-M distributed random variable. Although this method could also be used for M > 3, the former techniques are computationally much more efficient. The first method executes about 20 times faster, while the second method executed from 7 to 20 times faster dependent on the value for M.

48

5.3 Effect of Ionospheric Scintillation on Signal to Noise Ratio

The value for B obtained from Subroutine NAKGMI is used in Eqn. (5-3) to determine G which is in turn used to modify the signal to noise ratio (SNR) as shown in Eqns. (3-9) and (3-10) of Section 3.2.1. Because SNR is a function of power rather than amplitude, a G^4 term appears in place of the G^2 term of Eqn. (5-2).

5.4 Calculation of Traverse Angle Fluctuations

The traverse angle fluctuations are obtained by combining the output of subroutine Gauss, which generates an N(0,1) Gaussian random number, and Eqn. (5-9) for σ_T. We then obtain the traverse angle fluctuation (in radians), Δ_{Trav}, as

$$\Delta_{Trav} = (\frac{\pi}{180}) \ .04 \ \sigma_G \ RN(\tau) \tag{5-13}$$

$$= .6981 \times 10^{-3} \ \sigma_G \ RN(\tau) \tag{5-14}$$

where $RN(\tau)$ is an N(0,1) Gaussian random number, and the τ is used to denote that the particular random number sample is held for τ seconds before being replaced by another sample.

The azimuth fluctuation, ΔA_{Sint}, becomes

$$\Delta A_{Sint} = \Delta_{Trav}/\cos(E) \tag{5-15}$$

where E is the elevation of the target. If the radar is a phased array, then

49

the azimuth angle fluctuations are transformed into fluctuations in U and V coordinates by the transformation

$$\Delta U_{Sint} = -\cos(E) \cos(A-AZ) \Delta A_{Sint}$$

$$\Delta V_{Sint} = \cos(E) \sin(A-AZ) \sin(EL) \Delta A_{Sint}$$

where ΔU_{Sint} and ΔV_{Sint} are the fluctuations in U and V, respectively, AZ and EL are the boresite azimuth and elevation directions of the phased array, and A is the azimuth of the target.

6.0 MULTIPATH ERRORS

Multipath errors are considered to be a result of two interfering paths for the return from a target. The first path is a direct return to the main-lobe of the beam. The second path is an indirect return due to reflection from the earth's surface into a sidelobe of the beam (see Fig. 6-1). Note that this formulation is not intended to model multipath errors in the main beam at low elevation angles. The latter type of multipath gives rise to much greater error magnitudes.

6.1 Multipath Sidelobe Level Model

The sidelobe level multipath error is primarily an angle error. The total amplitude of the return is insignificantly affected by the sidelobe portion of the incoming signal, which is severely attenuated by the sidelobe level and ground reflection. However, this small signal is still sufficient to cause substantial pointing errors in the angle tracking loop.

A detailed treatment of the multipath problem is available in Barton [15] from which the following model is obtained. We start by assuming a monopulse radar pointing at a target with elevation angle Θ_t. If the sum and difference channels are denoted by Σ and Δ, respectively, then the effect of the reflected signal is to generate a spurious output in the Δ-channel which gives rise to an rms elevation error of

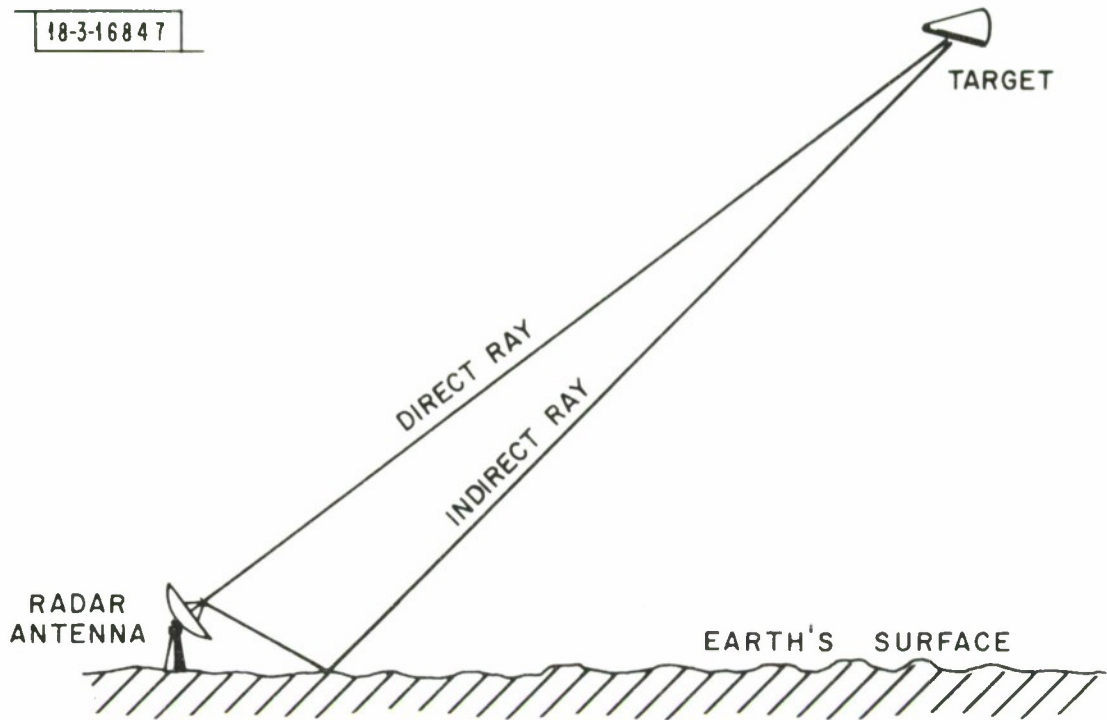$$\sigma_{EM} = \frac{\rho \, \Theta_{bw}}{k_m \sqrt{2} \, SLL} \tag{6-1}$$

51

Fig. 6.1. Multipath errors due to direct and reflected returns from
the target.

where θ_{bw} is the 3 db elevation mainlobe beamwidth, ρ the reflection coefficient at the reflection point on the earth's surface, and k_m the normalized monopulse Δ pattern slope. SLL is the Σ mainlobe to Δ sidelobe voltage ratio averaged over the first Fresnel zone nominally centered $2\theta_t$ below the mainlobe axis [see ref.[15], figure 2].

The program obtains SLL from a pre-stored table which depends on the particular type of radar which is being simulated. ρ is calculated as

$$\rho = |R_i| p \, D \qquad (6\text{-}2)$$

where

R_i - is the reflection coefficient from a flat surface for the received polarization given by equations (6-3) to (6-5).

D - is the divergence to account for the earth's curvature.

p - is the surface roughness factor. It is given by $p=\exp\{-4\pi\Delta\sin E\}$ where Δ is the mean surface roughness in wavelengths.

E - elevation angle.

The reflection coefficient for the various types of polarizations are as follows:

vertical $\qquad R_V = \dfrac{\varepsilon \, \sin E - \sqrt{\varepsilon - \cos^2 E}}{\varepsilon \, \sin E + \sqrt{\varepsilon - \cos^2 E}} \qquad (6\text{-}3)$

horizontal $\qquad R_H = \dfrac{\sin E - \sqrt{\varepsilon - \cos^2 E}}{\sin E + \sqrt{\varepsilon - \cos^2 E}} \qquad (6\text{-}4)$

circular $\qquad |R_c| = \tfrac{1}{2}[\,|R_V|^2 + |R_h^2| + 2|R_V| \, |R_h|\cos(\phi_h - \phi_V)\,] \qquad (6\text{-}5)$
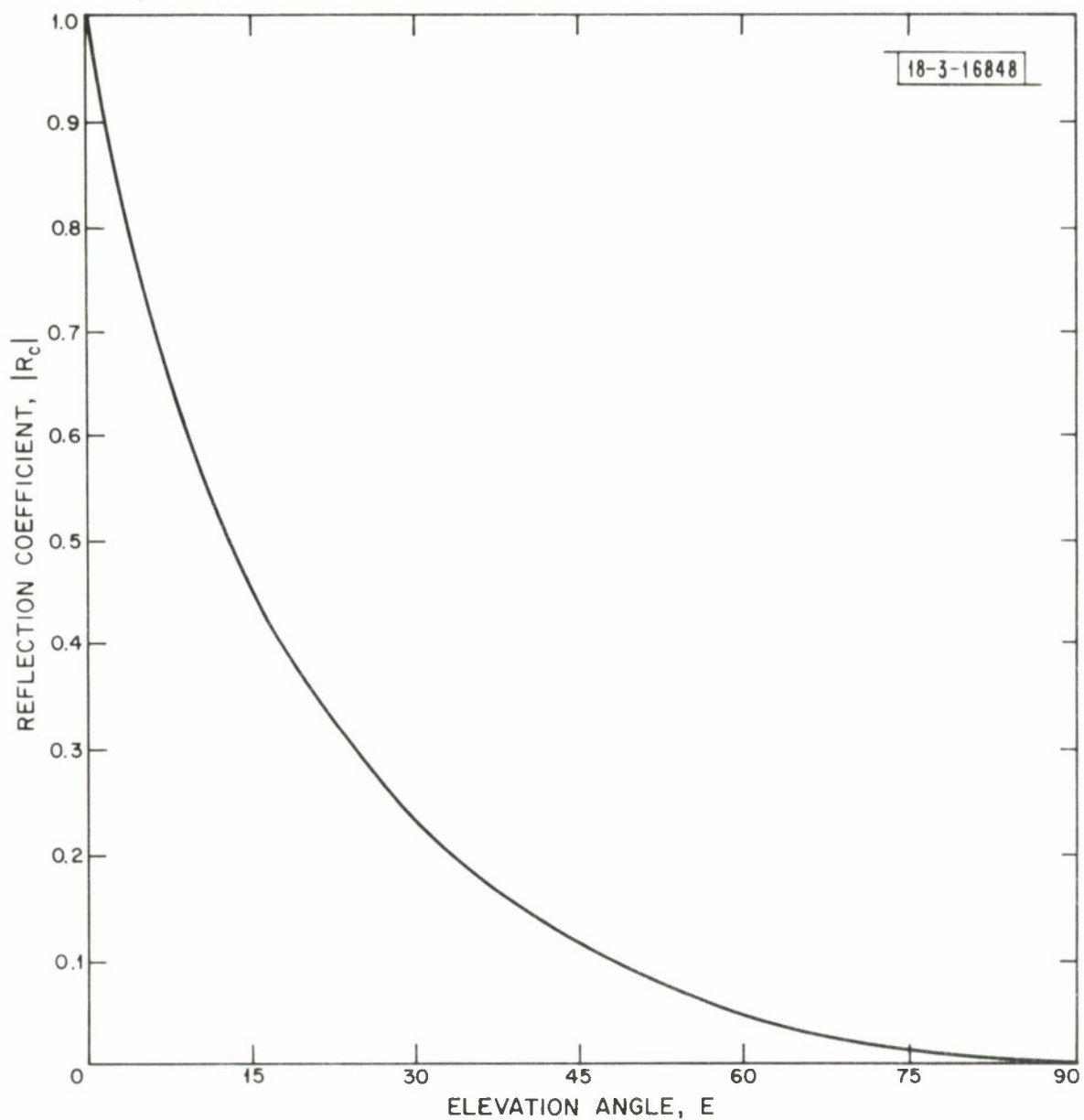
53

Fig. 6.2. Reflection coefficient for circular polarization, $|R_c|$, as a function of elevation angle ($\text{Re}(\varepsilon) = 10$, $\text{Im}(\varepsilon) = .018$).

where ε is the complex permittivity of the ground, and ϕ_v and ϕ_h are the phase lags on the reflection for vertical and horizontal polarization, respectively. Figure 6-2 shows $|R_c|$ as a function of elevation angle for the real part of the permittivity equal to 10, the imaginary part equal to 0.018, and a flat smooth surface.

If we denote the multipath elevation error by ΔE_{Mul} then

$$\Delta E_{Mul} = \sigma_{EM} \, RN(\Delta E) \tag{6-6}$$

where RN is zero mean unit variance Gaussian random number and the notation ΔE indicates that a new sample is obtained when the elevation angle changes by an amount ΔE. The value for ΔE is selected as half the mainlobe width, so that these errors remain correlated as long as the multipath error is due to interference from a particular sidelobe. For a new sidelobe, then a new random number sample is selected.

For a phased array radar the elevation angle errors must be transformed into U and V coordinates by the following expression

$$\Delta U_{Mul} = \sin(E) \, \sin(A-AZ) \Delta E_{Mul}$$

$$\Delta V_{Mul} = [\sin(E) \, \sin(EL) \, \cos(A-AZ) + \cos(E) \, \sin(EL)] \Delta E_{Mul}$$

where ΔU_{Mul} and ΔV_{Mul} are multipath errors in U and V respectively, AZ and EL are the boresite azimuth and elevation directions of the phased array, and E the elevation of the target.

55

6.2 Calculation of Multipath Errors

The reflection coefficient magnitude, R, and the rms sidelobe level values, SLL, are stored in ARIES as arrays which are functions of the elevation angle. See Tables 6-1 and 6-2.

The stored sidelobe level table is based on a mainlobe beamwidth of .5°. For other values of mainlobe beamwidth, BW, we define a scaled elevation angle E' as

$$E' = \frac{E}{2BW}$$

and then do a SLL table lookup using E' in place of E. For any value of $E' > 90°$, the sidelobe level table entry at 90° is used. Note also that the sidelobe level table (and this model) are applicable only when the elevation angle is greater than twice the mainlobe beamwidth. The reflection coefficient used is identical to the curve in Fig. 6-1 since $\Delta=0$, D=1 are assumed for the stored tables.

In operation table look-ups are made to obtain both ρ and the rms sidelobe level. These are combined with k_m and Θ_{BW} to form the σ_{EM} of Eqn. (6-1). Then the value of σ_{EM} obtained is multiplied by the same random sample used on the previous multipath calculation unless the elevation angle has changed by half a mainlobe beamwidth, in which case a new random number sample is selected.

The value selected for k_m depends on the exact type of radar used. For example, a monopulse radar might typically have a value for $k_m = 1.44$ and thus

$$\sigma_{EM} = \frac{R \; \Theta_{BW}}{1.44 \; 2 \; SLL}$$

$$= \frac{.491 \; R \; \Theta_{BW}}{SLL}$$

where σ_{EM} and Θ_{BW} are expressed in radians by ARIES.

Elevation (mr)	Reflection Coefficient
8.727	.96883000
34.907	.88430000
61.087	.81100000
87.266	.74674000
113.446	.68984000
139.626	.63905000
165.806	.59337000
191.986	.55203000
218.166	.51440000
244.346	.47999000
287.979	.42867000
331.613	.38364000
375.246	.34380000
418.879	.30828000
462.512	.27642000
506.145	.24772000
549.779	.22176000
593.412	.19819000
637.045	.17675000
680.678	.15721000
724.312	.13937000
794.125	.11399000
881.391	.08702700
968.658	.06463000
1055.924	.04619800
1134.464	.03262000
1221.730	.02055900
1308.997	.01143200
1396.263	.00504200
1483.530	.00127450
1570.796	.00027296

Table 6-1. Reflection coefficient, R, as a function of elevation angle (Re(ε) = 10, Im(ε) = .018, Δ = 0, D = 1).

Elevation (mr)	Sidelobe Level (dB)
17.453	-22.42
18.326	-23.53
19.199	-24.61
20.071	-25.78
20.944	-26.92
21.817	-28.00
34.907	-28.00
34.907	-33.98
104.720	-33.98
104.720	-40.00
174.533	-40.00
349.066	-40.00
523.599	-40.00
698.132	-40.00
872.665	-40.00
1047.198	-40.00
1570.796	-40.00

Table 6-2. Tables stored by ARIES for the RMS sidelobe level table as a function of elevation angle.

7.0 RADAR CROSS SECTION COMPUTATION

The purpose of this Section is to present a summary of the radar cross section (RCS) computation performed in the ARIES Program.

The ARIES program gives the user the option of selecting one of four methods for computing the RCS of each target. The first method of determining the RCS value is to do a table look-up on a set of stored static pattern tables in which each table represents the radar static pattern of a specified object. The other three methods of determining the RCS are based on mathematical models which represent a cylinder with end plates, a sinusoidally changing RCS with given frequency and null depth, and a sphere (constant RCS). The four options provide extreme flexibility in the type of analysis which can be performed with the ARIES program.

Two of the above options, the table look-up and cylinder, require the radar aspect and roll angles to the target to be determined before the RCS can be computed. Since the target motion is assumed to have six degrees of freedom, Euler's equation must be solved to determine the object's rotational motion about its center of mass. A coordinate transformation is then performed which permits the computation of radar aspect and roll angles from Eulerian angles, target state vector position and radar site location. In the following sections we will present a summary of the methods used to compute the radar aspect angle, roll angle and target radar cross section.
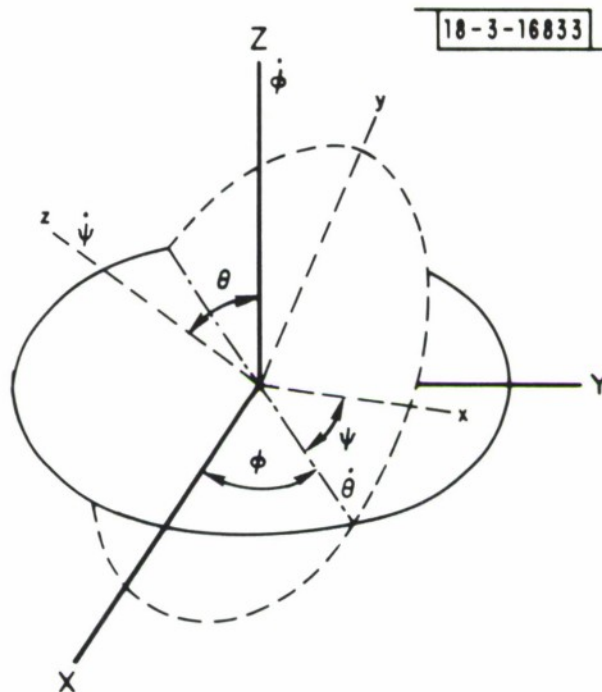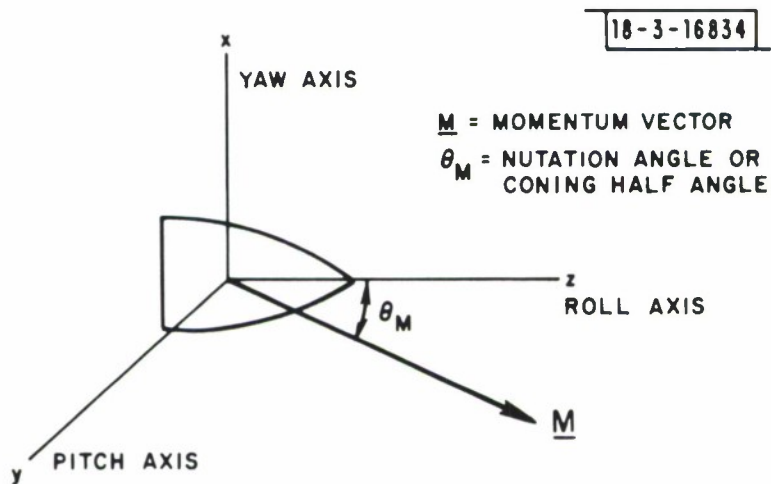
Fig. 7.1. Definition of Eulerian Angles.

Fig. 7.2. Definition of Object Body Axis.

7.1 Eulerian Angles

The Eulerian angles are defined by Fig. 7-1 in which (x y z) is obtained from (X Y Z) by a counterclockwise rotation first, about the Z axis by an angle ϕ, then about the x axis by an angle θ, and then about the z axis by an angle ψ. The transformation between the coordinate set $\underline{X} = (X,Y,Z)$ and $\underline{x} = (x,y,z)$ is given by

$$x = \overline{A}\underline{X} \tag{7-1}$$

and conversely

$$X = \overline{A}^{-1}\underline{x} = \overline{A}^{T}\underline{x} \tag{7-2}$$

where the matrix $\overline{A}$ is defined by

$$\overline{A}(\theta,\phi,\psi) = \begin{bmatrix} \cos\psi\cos\phi-\cos\theta\sin\phi\sin\psi & \cos\psi\sin\phi+\cos\theta\cos\phi\sin\psi & \sin\psi\sin\theta \\ -\sin\psi\cos\phi-\cos\theta\sin\phi\cos\psi & -\sin\psi\sin\phi+\cos\theta\cos\phi\cos\psi & \cos\psi\sin\theta \\ \sin\theta\sin\phi & -\sin\theta\cos\phi & \cos\theta \end{bmatrix} \tag{7-3}$$

In the application considered here, $\underline{x}$ denotes the principal body axis of the rotating body and $\underline{X}$ is an inertial frame. Note that $\overline{A}^{-1} = \overline{A}^{T}$ since the matrix $\overline{A}$ is orthogonal.

7.2 Coordinate Systems

The program uses several coordinate systems in which different functions are performed or measured. In this section we will establish relationships among all the coordinate systems used in the RCS portion of the program.

7.2.1 Principal Body Axes

The principal body axes are defined as a right-handed system whose origin is the center of mass of the object. This set of axes is attached to the object and assumed to be rotating with it. Definitions of the object body axis and rotational parameters are given in Fig. 7-2.

7.2.2 Local Horizontal

One set of the input parameters specified in the ARIES program are the Euler angles which give the initial orientation of the body axis with respect to the local horizontal. In this case, the local horizontal is defined as a right-handed system with the Z-axis along the velocity vector and Y-axis normal to the trajectory plane.

This coordinate frame is specified using the inertial state vector of the object at the initial time $t = t_o$. The axes of the local horizontal are obtained as follows:

The initial velocity vector and displacement vector are normalized:

$$V = (\dot{X}_I^2 + \dot{Y}_I^2 + \dot{Z}_I^2)^{\frac{1}{2}}$$

$$\begin{bmatrix} h_{ZX} \\ h_{ZY} \\ h_{ZZ} \end{bmatrix} = \begin{bmatrix} \dot{X}_I/|V| \\ \dot{Y}_I/|V| \\ \dot{Z}_I/|V| \end{bmatrix} \qquad (7\text{-}4)$$

$$|R| = (X_I^2 + Y_I^2 + Z_I^2)^{\frac{1}{2}}$$

$$\begin{bmatrix} h_{RX} \\ h_{RY} \\ h_{RZ} \end{bmatrix} = \begin{bmatrix} X_I/|R| \\ Y_I/|R| \\ Z_I/|R| \end{bmatrix} \tag{7-5}$$

where the subscript I indicates a component in the ECI frame. Note that $\underline{h}_Z$ and $\underline{h}_R$ are in the trajectory plane.

We now define the local horizontal Y direction as normal to the trajectory plane.

$$H_Y = \underline{h}_Z \times \underline{h}_R$$

$$\begin{bmatrix} H_{YX} \\ H_{YY} \\ H_{YZ} \end{bmatrix} = \begin{bmatrix} h_{ZY}\, h_{RZ} - h_{RY}\, h_{ZZ} \\ h_{ZZ}\, h_{RY} - h_{RZ}\, h_{ZX} \\ h_{ZX}\, h_{RY} - h_{RX}\, h_{ZY} \end{bmatrix} \tag{7-6}$$

Normalizing Eqn. (7-6) we obtain:

$$|H| = (H_{YX}^2 + H_{YY}^2 + H_{YZ}^2)^{\frac{1}{2}}$$

$$\begin{bmatrix} h_{YX} \\ h_{YY} \\ h_{YZ} \end{bmatrix} = \begin{bmatrix} H_{YX}/|H| \\ H_{YY}/|H| \\ H_{YZ}/|H| \end{bmatrix} \tag{7-7}$$

The final step is to define the local horizontal X axis as

$$\underline{h}_X = \underline{h}_Z \; X(-\underline{h}_Y)$$

$$\begin{bmatrix} h_{XX} \\ h_{XY} \\ h_{XZ} \end{bmatrix} = \begin{bmatrix} h_{YY} \, h_{ZZ} - h_{ZY} \, h_{YZ} \\ h_{YZ} \, h_{ZX} - h_{ZZ} \, h_{YX} \\ h_{YX} \, h_{ZY} - h_{ZX} \, h_{YY} \end{bmatrix} \tag{7-8}$$

Note that $\underline{h}_X$ is a unit vector since $\underline{h}_Z$ and $\underline{h}_Y$ are orthogonal.

The transformation matrix which takes the initial local horizontal into inertial space is obtained by using Eqns. (7-4), (7-7) and (7-8). The matrix is as follows:

$$\overline{V} = \begin{bmatrix} h_{XX} & h_{XY} & h_{XZ} \\ h_{YX} & h_{YY} & h_{YZ} \\ h_{ZX} & h_{ZY} & h_{ZZ} \end{bmatrix} \tag{7-9}$$

7.3   Rotational Motion of a Rigid Body

The rotational motion of a rigid body with no external torques applied is given by the solution of the homogeneous form of Euler's equations. This solution leads directly to the determination of the time varying Euler angles between body axis of the object and an inertial frame. In this section we present a summary of the method used in the ARIES Program to solve for the rotational motion.

7.3.1 Equations of Motion

The absolute motion of a body is described in terms of the orientation of the principal body axes (x,y,z) with respect to an inertial coordinate frame (X,Y,Z). If $(\omega_x, \omega_y, \omega_z)$ are the components of angular velocity of the body in the (x,y,z) frame, then the angular velocity vector, $\underline{\Omega}$, and the momentum vector, $\underline{M}$, in the (x,y,z) frame can be written as

$$\underline{\Omega} = \begin{bmatrix} \omega_x \\ \omega_y \\ \omega_z \end{bmatrix} \qquad \underline{M} = \begin{bmatrix} I_x \omega_x \\ I_y \omega_y \\ I_z \omega_z \end{bmatrix}$$

where I_x, I_y and I_z are the principal moments of inertia of the body. For the exoatmospheric portion of the trajectory, it is assumed that there are no external torques applied to the body. This implies that angular momentum is conserved, that is

$$\left(\frac{d\underline{M}}{dt} \right)_{(xyz)} + \underline{\Omega} \times \underline{M} = 0 \tag{7-10}$$

which is the vector form of Euler's equations. In component form Eqn. (7-10) becomes

$$\dot{\omega}_x = -\left(\frac{I_z - I_y}{I_x}\right)\omega_y\omega_z$$

$$\dot{\omega}_y = \left(\frac{I_z - I_x}{I_y}\right)\omega_x\omega_z \qquad\qquad\qquad (7\text{-}11)$$

$$\dot{\omega}_z = \left(\frac{I_y - I_x}{I_z}\right)\omega_x\omega_y$$

Two integrals of Euler's equations are known from the laws of conservation of energy and angular momentum:

$$I_x\omega_x^2 + I_y\omega_y^2 + I_z\omega_z^2 = 2E$$

$$I_x^2\omega_x^2 + I_y^2\omega_y^2 + I_z^2\omega_z^2 = M^2$$

where

$$2EI_x < M^2 < 2EI_z \text{ for } I_x < I_y < I_z$$

or where

$$2EI_x > M^2 > 2EI_z \text{ for } I_x > I_y > I_z$$

in which the energy E and the magnitude M of the angular momentum are given constants.

Manipulation of Euler's equations and the equations for E and M^2 will give uncoupled equations for (ω_x, ω_y, ω_z) which may be solved in terms of Jacobian elliptic functions. In some cases a more trivial solution may be

obtained depending upon the relative magnitudes of the principal moments of inertia (I_x, I_y, I_z) and whether $M^2 > 2EI_y$ or $M^2 < 2EI_y$. For the details of the solution the reader is referred to references [16] and [17].

7.3.2 Motion in Space

Using the calculated angular velocity (ω_x, ω_y, ω_z) obtained from the solution of Euler's equation, the motion of the body with respect to an inertial frame can be determined. This implies that we must determine the time varying Euler angles between the body axis and the inertial frame. To simplify the resulting equations one axis of the inertial system is selected to be along the invariant angular momentum vector $\underline{M}$. The inertial system is therefore defined to be the momentum frame taking the Z-axis in the direction of the constant $\underline{M}$ vector.

The components of angular velocity can be expressed in terms of the Eulerian angles and their derivatives, as

$$\left.\begin{array}{l} \omega_x = \dot{\phi}_M \sin\Theta_M \sin\psi_M + \dot{\Theta}_M \cos\psi_M \\[2mm] _y = \dot{\phi}_M \sin\Theta_M \cos\psi_M - \dot{\Theta}_M \sin\psi_M \\[2mm] _z = \dot{\phi}_M \cos\Theta_M + \dot{\psi}_M \end{array}\right\} \qquad (7\text{-}12)$$

where the subscript M denotes that the angles are taken with respect the inertial momentum frame.

The solution of Eulerian angles (Θ_M, ϕ_M, ψ_M) follows using the angular momentum equations. The polar angle and azimuth of the momentum Z-axis with

respect to the body axes x, y, z are respectively θ_M and $\frac{1}{2}\pi - \psi_M$ and we obtain on taking the components of $\underline{M}$ along the axes x, y, z the expressions:

$$\left.\begin{aligned}
|\underline{M}| \, \sin\theta_M \, \sin\psi_M &= I_x \omega_x(t) \\
|\underline{M}| \, \sin\theta_M \, \cos\psi_M &= I_y \omega_y(t) \\
|\underline{M}| \, \cos\theta_M &= I_z \omega_z(t).
\end{aligned}\right\} \tag{7-13}$$

Hence

$$\left.\begin{aligned}
\cos\theta_M(t) &= I_z \omega_z(t)/|\underline{M}| \\
\tan\psi_M(t) &= I_x \omega_x(t)/I_y \omega_y(t)
\end{aligned}\right\} \tag{7-14}$$

which give the angles θ_M and ψ_M as a function time.

The angle ϕ_M does not appear in Eqn. (7-13) and to calculate it use Eqn. (7-12), which expresses the components of ω in terms of the time derivatives of the Eulerian angles. Eliminating $\dot{\theta}_M$ from Eqn. (7-12), then using Eqn. (7-13) we obtain

$$\dot{\phi}_M = \frac{|M| (I_x \omega_x^2 + I_y \omega_y^2)}{(I_x \omega_x^2 + I_y \omega_y^2)} \tag{7-15}$$

The function $\phi_M(t)$ is obtained by integrating Eqn. (7-15).

7.3.3 Initial Euler Angles to Momentum Frame

From the foregoing result, define the initial Euler angles between the momentum frame and the body axes at t_o as

$$\theta_M(t_o) = \cos^{-1}\left[I_z\omega_z(t_o)/|M|\right]$$

$$\psi_M(t_o) = \tan^{-1}\left[I_x\omega_x(t_o)/I_y\omega_y(t_o)\right] \qquad (7\text{-}16)$$

$$\phi_M(t_o) = 0.$$

The transformation from body axes to the momentum frame at t_o is given by

$$\underline{X} = \overline{A}^T[\theta_M(t_o),\ \phi_M(t_o),\ \psi_M(t_o)]\underline{x} \qquad (7\text{-}17)$$

where $\overline{A}$ is the matrix defined in Eqn. (7-3).

7.4   Initial Conditions

The following initial parameters are required in order to define a solution to Euler's equations. The parameters are the three rotational rates $(\omega_x,\ \omega_y,\ \omega_z)$, the three moments of inertia $(I_x,\ I_y,\ I_z)$ around the principal body axes, and three Euler angles $(\theta_i,\ \phi_i,\ \psi_i)$ which relate the initial body axis to the local horizontal. The initial Euler angles between the momentum frame and the principal body axes are given by Eqn. (7-16).

The solution to Euler's equation is obtained using the method outlined in reference [16].

7.5   Radar Aspect and Roll Angle

From the foregoing results we are now in a position to define an overall transformation between the principal body axes and inertial space from which the radar aspect and roll angle can be computed. The transformation is shown below. Using Eqns. (7-1), (7-3), (7-9) and (7-17) we obtain:

$$\underline{X} = \overline{V} \ \overline{A}^T[\Theta_i, \phi_i, \psi_i]\overline{A}[\Theta_M(t_o), \phi_M(t_o), \psi_M(t_o)]\overline{A}^T[\Theta_M(t), \phi_M(t), \psi_M(t)]\underline{x}$$

$$\underline{X} = \overline{T}\underline{x} \tag{7-18}$$

This transformation can be diagramed as follows:
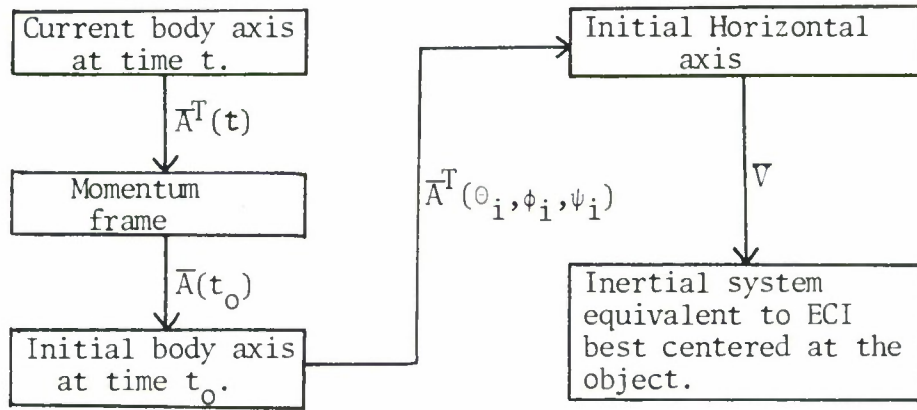
We can now determine the radar aspect and roll angles in the following manner. The aspect angle Θ_a, shown in Fig. 7-3, is defined as the angle between the radar line of sight and the re-entry vehicle (RV) roll or z-azis. That is

$$\Theta_a = \cos^{-1}\left[\frac{R_{SM} \ Z}{|R_{SM}|}\right] \tag{7-19}$$

where $\underline{R}_{SM}$ is the vector from the radar site to the RV.

$$\underline{R}_{SM} = (X_M - X_S, \ Y_M - Y_S, \ Z_M - Z_S) \tag{7-20}$$

and

(X_M, Y_M, Z_M) is RV coordinates in inertial space.

(X_S, Y_S, Z_S) is radar coordinates in inertial space.

$\underline{Z} = (Z_X, Z_Y, Z_Z)$ is the position of the roll or z-axis of the object in inertial space which is given by

$$\underline{Z} = \overline{T} \begin{bmatrix} 0 \\ 0 \\ 1 \end{bmatrix} \tag{7-21}$$

The roll angle, Θ_r, shown in Fig. 7-3, is defined by

$$\Theta_r = \tan^{-1} \left[\frac{R_{SM} \, \underline{X}}{R_{SM} \, \underline{Y}} \right] \tag{7-22}$$
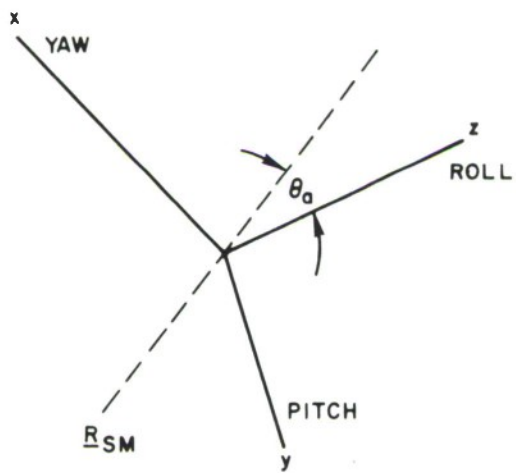
where

$\underline{\dot{Y}} = (Y_X, Y_Y, Y_Z)$ is the position of the pitch axis in the inertial system, that is

$$\underline{Y} = \overline{T} \begin{bmatrix} 0 \\ 1 \\ 0 \end{bmatrix} \tag{7-23}$$

$\underline{X} = (X_X, X_Y, X_Z)$ is the position of the yaw axis in the inertial system, that is

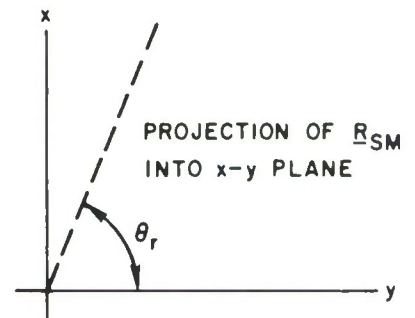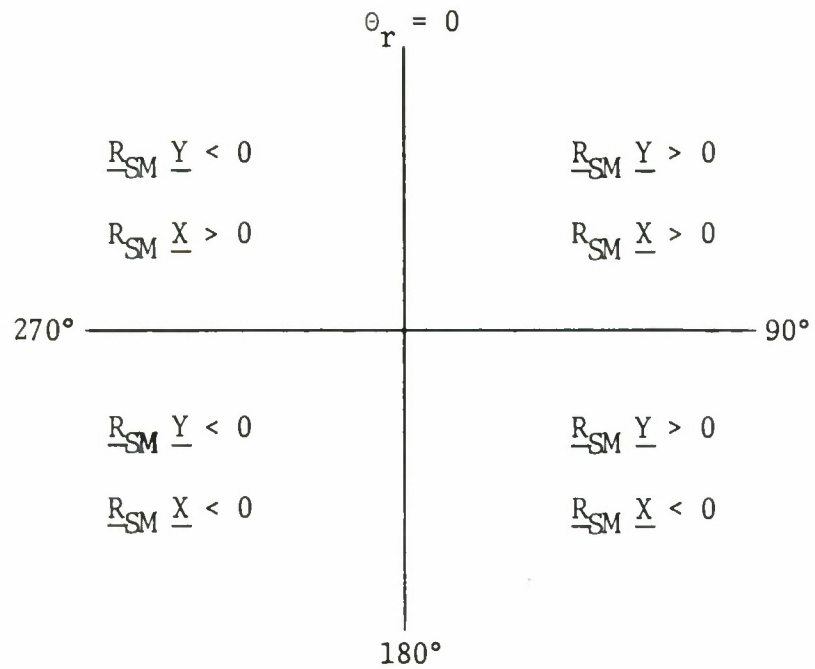$$\underline{X} = \overline{T} \begin{bmatrix} 1 \\ 0 \\ 0 \end{bmatrix} \tag{7-24}$$

72

Fig. 7.3. Definition of Aspect Angle, θ_a, and Roll Angle, θ_r.

The quadrant in which Θ_r lies is determined from the signs of the numerator and denominator of Eqn. (7-22), according to the following convention.

$$\Theta_r = 0$$

$\underline{R}_{SM} \, \underline{Y} < 0$	$\underline{R}_{SM} \, \underline{Y} > 0$
$R_{SM} \, \underline{X} > 0$	$R_{SM} \, \underline{X} > 0$

270° ———————————|——————————— 90°

$\underline{R}_{SM} \, \underline{Y} < 0$	$\underline{R}_{SM} \, \underline{Y} > 0$
$\underline{R}_{SM} \, \underline{X} < 0$	$\underline{R}_{SM} \, \underline{X} < 0$

180°

7.6 Radar Cross Section

The radar cross section can be computed by one of four methods. The methods will be described here. The value for RCS computed by any one of these methods is used in Eqns. (3-8) and (3-9) to determine the signal to noise ratio of the target.

7.6.1 Static Pattern

Static pattern table look up is used when RCS input option 1 or 2* is selected. The static pattern table consists of measured narrow-band radar cross section data with two orthogonal polarization components. The tables are constructed by processing the measured data to eliminate points which can be fitted by linear interpolation between adjacent points. Maximum table size is 25 roll cuts with 400 aspect points per roll cut. To reduce core storage requirements for the tables, the 400 aspect data points are each truncated to 12 binary bits in accuracy and packed 5 points per 60-bit word. In this way up to 4 tables can be kept core resident during a simulation run.

The program does a static pattern table look up for each specified table type using the aspect and roll angles computed in Section 7.5. Since many targets are symmetric in some way, the aspect and roll angles are converted to an appropriate interval for the specified table. All roll and aspect angles are first transformed to the interval

---

*Input option 2 is not currently implemented.

$$-180^\circ \leq \Theta_a \leq 180^\circ$$

$$0 \leq \Theta_r \leq 180^\circ$$

(7-25)

and then transformed to the interval for the symmetry of the target according to table 7-1.

Symmetry Code	Range of Θ_a	Range of Θ_r
1	$(-180^\circ, +180^\circ)$	$(0, 180^\circ)$
2	$(0^\circ, 180^\circ)$	$(0, 90^\circ)$
3	$(-180^\circ, +180^\circ)$	$(0, 90^\circ)$
4	$(0^\circ, 180^\circ)$	$(0, 45^\circ)$
5	$(0^\circ, 180^\circ)$	$(0, 40^\circ)$
6	$(-180^\circ, +180^\circ)$	$(0, 45^\circ)$
7	$(-180^\circ, +180^\circ)$	(0)
8	$(0, 90^\circ)$	(0)

TABLE 7-1

SYMMETRY RANGES

7.6.2 Cylinder With End Plates

A target with RCS input option 3 selected is modelled as a cylinder with end plates. This option provides the capability of simulating the dynamic motion of a tank without the need for a table look up. The radar cross section is computed using the following expression

$$
RCS = \frac{r\lambda \, \sin\Theta_a}{2\pi} \left[\frac{\sin(k \, \ell \, \cos\Theta_a)}{\cos\Theta_a}\right]^2
$$

$$
+ \pi r^2 \cot^2\Theta_a \, J_1^{\,2}(2kr \, \sin\Theta_a) \qquad\qquad (7\text{-}26)
$$

where

r = cylinder radius

ℓ = cylinder length

Θ_a = aspect angle

J_1 = first-order Bessel function

λ = radar transmitting wavelength

k = $2\pi/\lambda$

Note that the first term in Eqn. (7-26) gives the scattering from the cylindrical surface while the second gives the scattering from an end plate.

The RCS for both left and right circular polarizations are set equal to RCS in Eqn. (7-26). A plot of Eqn. (7-26) as a function of aspect angle for a given ℓ, r and λ is shown in Fig. 7-4.
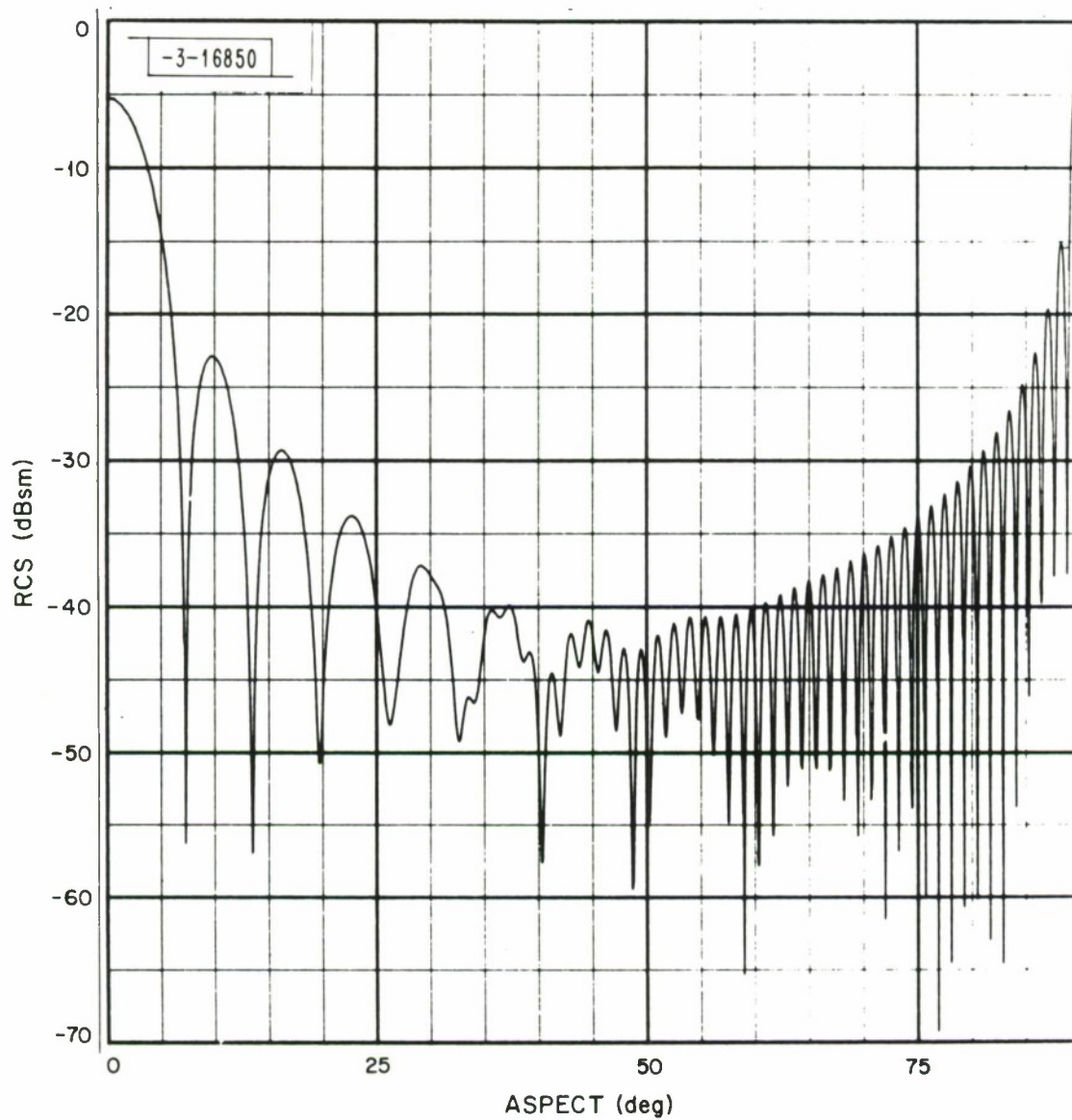
77

Fig. 7.4. Radar Cross Section of cylinder with end plate where
r = 4.115 cm, ℓ = 20.894 cm, λ = .8611 cm.

7.6.3 Sinusoidal RCS

The radar cross section for RCS input option 4 is a sinusoidal function of time. This can be used to simulate the rotational motion of symmetric objects without requiring static pattern tables. The functional form of the RCS for both right circular and left circular polarization is given by the expression below:

$$RCS = \frac{A}{2}[1 + (1-R_f)\sin(\omega t) + R_f] \qquad (7-27)$$

where

A = peak RCS amplitude

R_f = null amplitude/A

ω = RCS scintillation rate in rad/sec.

Note that input parameters for this option enter the sinusoid peak and sinusoid null in dbsm. The values for A and R_f in Eqn. (7-27) are computed from these values.

7.6.4 Spherical Target

RCS option 5 specifies that the radar cross section is a constant. The RCS amplitude of both right circular and left circular polarization is set to the value specified by the input parameter.

7.7 RCS Data Tape

An Edit option in the ARIES Program permits the user to write a magnetic tape containing the measured radar cross section history for each target during every track segment. The measured radar cross section of the target is computed using the true RCS, an ionospheric scintillation term and measured target range. This value effectively represents the RCS a radar system would compute from received signal. The object of writing a tape of this type is to permit offline processing and analysis of target signature data.

The expression used in computing the measured right and left circular polarization RCS is

$$RCS_M = \left[\frac{R_M}{R_T}\right]^4 \ RCS_i \ G^4 \tag{7-28}$$

where

$\quad R_M$ = measured range of target

$\quad R_T$ = true range of target

$\quad RCS_i$ = radar cross section of target computed according to Section 7.5 where i=1 represents right circular polarization and i=2 left circular polarization

$\quad G$ = ionospheric scintillation term given by Eqn. (5-3)

The complete form of the RCS data tape is given in Section 4.11.3 of reference [1].

80

ACKNOWLEDGMENT

References

1. M.E. Austin, "The ARIES Program: A General Overview and Users' Guide," Technical Note 1975-14, Lincoln Laboratory, M.I.T. (to be published).

2. B.L. Diamond and M.E. Austin, "The ARIES Program: Coordinates, Transformations, Trajectories and Tracking," Technical Note 1975-15, Lincoln Laboratory, M.I.T. (to be published).

3. G.B. Morse and W.E. Courtney, "Applications and Results," private communication.

4. D.E. Kerr, Propagation of Short Radar Waves, Radiation Laboratory Series, Vol. 13, (McGraw-Hill, New York, 1951).

5. C.F. Campen and A.E. Coles, "Tropospheric Variations of Refractive Index at Microwave Frequencies," Air Force Surveys in Geophysics No. 79, Geophysical Research Directorate (October 1955).

6. E.K. Smith and S. Weintraub, "The Constants in the Equation for Atmospheric Refractive Index at Radio Frequencies," Central Radio Propagation Laboratory, Natl. Bur. Stand. Report No. 1938 (September 1952).

7. B.R. Bean and E.J. Dutton, Radio Meteorology, Natl. Bur. Stand. Monograph 22 (1966).

8. S.K. Mitra, The Upper Atmosphere (The Asiatic Society of Calcutta, 1952).

9. B.R. Bean and G.D. Thayer, "Comparison of Observed Atmospheric Radio Refraction Effects with Values Predicted Through the Use of Surface Weather Observations," J. Res. Natl. Bur. Stand. 67D, 3, 273-285 (1963).

10. B.R. Bean, B.A. Cahoon, and G.D. Thayer, "Tables for the Statistical Prediction of Radio Ray Bending and Elevation Angle Errors Using Surface Values of the Refractive Index," Natl. Bur. Stand. TN44 (1960).

11. A.R. Harris, "Azimuthal Refraction - A Study of Atmospheric Properties Affecting Radar Accuracy," General Electric Report (February 1957).

12. R.H. Wand, private communication from R.H. Wand to W.E. Courtney, "Worst-Case Models for Ionospheric Scintillation" (23 April 1974).

13. M. Nakagami, "A General Formulation of Intensity Distribution of Rapid Fading," in Statistical Methods of Radio Wave Propagation, edited by W.C. Hoffman (Pergamon Press, New York, 1960), pp. 3-36.

References (Cont'd)

14. A.J. Thomasian, The Structure of Probability Theory with Applications (McGraw-Hill, New York, 1969), pp. 427-428.

15. D.K. Barton, "Low Angle Radar Tracking," Proc. IEEE, 62, 687-704 (1974).

16. L.D. Landau and E.M. Lifshitz, Mechanics (Addison-Wesley, Reading, Massachusetts, 1960), pp. 105-124.

17. B.J. Burdick, "TUMBLE: A Dynamic Simulation Program," Project Report RMP-54, Lincoln Laboratory, M.I.T. (8 January 1975).

REPORT DOCUMENTATION PAGE		READ INSTRUCTIONS BEFORE COMPLETING FORM
1. REPORT NUMBER ESD-TR-75-222	2. GOVT ACCESSION NO.	3. RECIPIENT'S CATALOG NUMBER
4. TITLE *(and Subtitle)* The ARIES Program: Analysis and Generation of Simulated Radar Measurements		5. TYPE OF REPORT & PERIOD COVERED Technical Note
		6. PERFORMING ORG. REPORT NUMBER Technical Note 1975-16
7. AUTHOR(s) Mannos, James L. and Katz, Joseph L.		8. CONTRACT OR GRANT NUMBER(s) F19628-76-C-0002
9. PERFORMING ORGANIZATION NAME AND ADDRESS Lincoln Laboratory, M.I.T. P.O. Box 73 Lexington, MA 02173		10. PROGRAM ELEMENT, PROJECT, TASK AREA & WORK UNIT NUMBERS Project No. 8X363304D215 Program Element No. 63304A
11. CONTROLLING OFFICE NAME AND ADDRESS Ballistic Missile Defense Program Office Department of the Army 1320 Wilson Boulevard Arlington, VA 22209		12. REPORT DATE 9 July 1975
		13. NUMBER OF PAGES 90
14. MONITORING AGENCY NAME & ADDRESS *(if different from Controlling Office)* Electronic Systems Division Hanscom AFB Bedford, MA 01731		15. SECURITY CLASS. *(of this report)* Unclassified
		15a. DECLASSIFICATION DOWNGRADING SCHEDULE

16. DISTRIBUTION STATEMENT *(of this Report)*

Approved for public release; distribution unlimited.

17. DISTRIBUTION STATEMENT *(of the abstract entered in Block 20, if different from Report)*

18. SUPPLEMENTARY NOTES

None

19. KEY WORDS *(Continue on reverse side if necessary and identify by block number)*

ARIES Program	atmospheric refraction	multipath errors
radar measurements	ionospheric scintillation	radar cross section
radar noise		

20. ABSTRACT *(Continue on reverse side if necessary and identify by block number)*

This report describes the modeling of measurement errors in precision, long range tracking radars due to the combination of environmental effects and variations in target cross section. The environmental effects considered are tropospheric and ionospheric refraction and time delay, ionospheric scintillation, and multipath through the sidelobes at low tracking angles. In addition, radar errors due to thermal and galactic noise, equipment jitter, and bias are included. Six-degree-of-freedom vehicle dynamics are modeled to realistically represent the changing radar cross section due to target dynamics such as tumbling and precession.

DD FORM 1473 EDITION OF 1 NOV 65 IS OBSOLETE
1 JAN 73